Measurements of triple- and double-spin parameters in elastic p-p scattering at 6 GeV/c

I. P. Auer,[a] J. Chalmers,[b] E. Colton,[c] R. Giese,[d] H. Halpern,[e] D. Hill, R. Miller, K. Nield,[f] B. Sandler,[g] H. Spinka, N. Tamura,[h] D. Underwood, Y. Watanabe,[i] and A. Yokosawa
High Energy Physics Division, Argonne National Laboratory, Argonne, Illinois 60439

A. Beretvas[j] and D. Miller
Department of Physics, Northwestern University, Evanston, Illinois 60201
(Received 11 April 1985)

Toward the goal of experimentally determining the p-p elastic-scattering amplitudes at 6 GeV/c, we have measured a number of triple- and double-spin correlation parameters over the $|t|$ range between 0.2 and 1.0 (GeV/c)^2. These new data permit the first nucleon-nucleon amplitude determination in the multi-GeV energy range. Polarized beams from the Argonne Zero Gradient Synchrotron and polarized targets were utilized. The polarization of the recoil proton was measured with a carbon polarimeter. A total of 14 different spin observables were measured (five spin transfer, four depolarization, and five triple-spin correlation parameters). These have been combined with earlier results, resulting in a data set of typically 30 measurements of 20 different spin observables for each of six $|t|$ values between 0.2 and 1.0 (GeV/c)^2. A solution for the amplitudes has been found at each $|t|$, and comparisons are presented with several different models. The spin-nonflip helicity amplitudes are found to be much larger than the spin-flip amplitudes.

I. INTRODUCTION

A series of experiments were performed several years ago at 6 GeV/c laboratory momentum to determine experimentally the p-p elastic scattering amplitudes in the region of four-momentum transfer squared $|t|$ up to about 1.0 (GeV/c)^2. Most of these earlier measurements were performed with polarized proton beams from the Argonne National Laboratory Zero Gradient Synchrotron (ZGS). They included complicated triple-spin experiments,[1,2] with polarized beam and polarized target and a determination of the outgoing spin of one particle with a carbon polarimeter, as well as single- and double-spin measurements.[3–14] The difficult triple-spin experiments measured more than one spin observable simultaneously, and they used polarized proton targets with spin aligned perpendicular to the scattering plane. The rapidly falling p-p differential cross section at 6 GeV/c made high-precision measurements very difficult for $|t|$ above about 1.0 (GeV/c)^2.

This is a report on the last series of experiments carried out in the 6-GeV/c amplitude program. Polarized targets with spin aligned in the scattering plane were used. It has been shown that such measurements were needed to obtain uniquely the amplitudes in a model-independent fashion.[15] Results are presented for several triple-spin parameters, such as $H_{LSN}=(L,S;0,N)$ and $H_{NSS}=(N,S;0,S)$, and a number of double-spin parameters, such as $D_{SS}=(0,S;0,S)$ and $K_{LS}=(L,0;0,S)$. In some cases, mixtures of pure spin observables were obtained, such as $\tilde{D}_{LS}=(aD_{LS}+bD_{SS})$, where $D_{LS}=(0,L;0,S)$ and a and b are $|t|$-dependent constants. Some results from these experiments have been published previously.[12] Also, in some cases, the $|t|$ range was limited by the polarized-target magnet aperture.

Combining the data from these measurements with previous results[1–14] at 6 GeV/c gives up to 35 points and 21 different spin observables at some values of t. Roughly half of these are presented in this paper. As a consequence of the large number of spin observables, the amplitudes are highly overconstrained. Therefore, many checks for systematic errors are discussed.

In Sec. II we summarize the notation used for observables. Section III contains a description of the experimental apparatus; details of the methods used in data reduction are described in Sec. IV. We have used these new measurements to carry out a preliminary analysis of the p-p elastic-scattering amplitudes; the results are discussed briefly in Sec. V. The interpretations are given in Sec. VI, and the conclusions in Sec. VII.

II. FORMALISM

The general formalism has been presented in our previous paper[1] and is developed in the references cited therein. Spin directions for the beam, target, scattered, and recoil protons are shown in Fig. 1.

Expressions of spin parameters (beam, target; scattered, recoil) in the laboratory system are as follows:

$$P=(N,0;0,0)=(0,N;0,0)=(0,0;0,N)\ ,\ \text{polarization}\ ,$$

$$C_{ij}=(i,j;0,0)\ ,\ \text{spin-correlation parameters}\ ,$$

$$D_{ij}=(0,i;0,j)\ ,\ \text{depolarization parameters}\ ,$$

$$K_{ij}=(i,0;0,j)\ ,\ \text{polarization-transfer parameters}\ ,$$

$$H_{ijk}=(i,j;0,k)\ ,\ \text{triple-spin parameters}\ ,$$

where i, j, and k denote a direction of measured spin (N, L, or S).

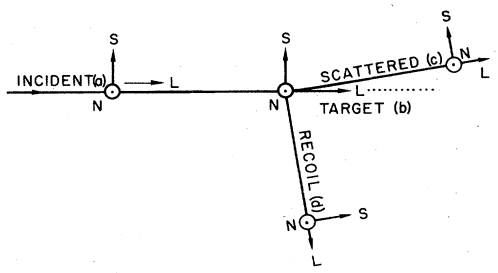

N: NORMAL TO THE SCATTERING PLANE
L: LONGITUDINAL DIRECTION
S = N x L IN THE SCATTERING PLANE

FIG. 1. Definition of spin directions.

The elastic-scattering amplitudes may be defined in many different ways; we have chosen two which are widely used. The t-channel-exchange amplitudes are defined so that each amplitude has definite quantum numbers at asymptotic energy;[16,17] these are N_0, N_1, and N_2 for natural-parity exchange and U_0 and U_2 for unnatural-parity exchange. The s-channel helicity amplitudes[18–21] may be expressed as follows:

$$\begin{aligned}
\langle ++|++\rangle &= \phi_1 , \\
\langle --|++\rangle &= \phi_2 , \\
\langle +-|+-\rangle &= \phi_3 , \\
\langle +-|-+\rangle &= \phi_4 , \\
\langle ++|+-\rangle &= \phi_5 .
\end{aligned} \tag{1}$$

The amplitudes ϕ_1 and ϕ_3 are net helicity nonflip, ϕ_2 and ϕ_4 are helicity double flip, and ϕ_5 is helicity single flip.

The t-channel-exchange amplitudes are then

TABLE I. Laboratory observables in terms of exchange amplitudes.

(a)

Observables $(B,T;S,R)$	Exchange amplitudes
(Single scattering)	
σ^{tot}	$4\pi/k\ \text{Im}N_0(0)$
$\Delta\sigma_L^{\text{tot}}$	$8\pi/k\ \text{Im}U_0(0)$
$\Delta\sigma_T^{\text{tot}}$	$-8\pi/k\ \text{Im}U_2(0)$
$\sigma=(0,0;0,0)$	$\lvert N_0\rvert^2+2\lvert N_1\rvert^2+\lvert N_2\rvert^2+\lvert U_0\rvert^2+\lvert U_2\rvert^2$
$P=(0,N;0,0)$	$-2\,\text{Im}[(N_0-N_2)N_1^*]/\sigma$
$=(N,0;0,0)$	
$C_{NN}=(N,N;0,0)$	$2\,\text{Re}(U_0U_2^*-N_0N_2^*+\lvert N_1\rvert^2)/\sigma$
$C_{SS}=(S,S;0,0)$	$2\,\text{Re}(N_0U_2^*-N_2U_0^*)/\sigma$
$C_{SL}=(S,L;0,0)$	$2\,\text{Re}[(U_0+U_2)N_1^*]/\sigma$
$C_{LL}=(L,L;0,0)$	$-2\,\text{Re}(N_0U_0^*-N_2U_2^*)/\sigma$
Note: $(d\sigma/dt=\sigma\pi/k^2)$	
(Double scattering)	
1. K_{jk} measurement	
$K_{NN}=(N,0;0,N)$	$-2\,\text{Re}(U_0U_2^*+N_0N_2^*-\lvert N_1\rvert^2)/\sigma$
$K_{SS}=(S,0;0,S)$	$\{-2\,\text{Re}[(U_2-U_0)N_1^*]\sin\theta_R-2\,\text{Re}(N_0U_2^*+N_2U_0^*)\cos\theta_R\}/\sigma$
$K_{SL}=(S,0;0,L)$	$\{2\,\text{Re}[(U_2-U_0)N_1^*]\cos\theta_R-2\,\text{Re}(N_0U_2^*+N_2U_0^*)\sin\theta_R\}/\sigma$
$K_{LS}=(L,0;0,S)$	$\{-2\,\text{Re}[(U_2-U_0)N_1^*]\cos\theta_R-2\,\text{Re}(N_0U_0^*+N_2U_2^*)\sin\theta_R\}/\sigma$
$K_{LL}=(L,0;0,L)$	$\{-2\,\text{Re}[(U_2-U_0)N_1^*]\sin\theta_R+2\,\text{Re}(N_0U_0^*+N_2U_2^*)\cos\theta_R\}/\sigma$
2. D_{jk} measurement	
$D_{NN}=(0,N;0,N)$	$(\lvert N_0\rvert^2+2\lvert N_1\rvert^2+\lvert N_2\rvert^2-\lvert U_0\rvert^2-\lvert U_2\rvert^2)/\sigma$
$D_{SS}=(0,S;0,S)$	$\{-2\,\text{Re}[(N_0+N_2)N_1^*]\sin\theta_R-(\lvert N_0\rvert^2-\lvert N_2\rvert^2-\lvert U_0\rvert^2+\lvert U_2\rvert^2)\cos\theta_R\}/\sigma$
$D_{SL}=(0,S;0,L)$	$\{2\,\text{Re}[(N_0+N_2)N_1^*]\cos\theta_R-(\lvert N_0\rvert^2-\lvert N_2\rvert^2-\lvert U_0\rvert^2+\lvert U_2\rvert^2)\sin\theta_R\}/\sigma$
$D_{LS}=(0,L;0,S)$	$\{-2\,\text{Re}[(N_0+N_2)N_1^*]\cos\theta_R+(\lvert N_0\rvert^2-\lvert N_2\rvert^2+\lvert U_0\rvert^2-\lvert U_2\rvert^2)\sin\theta_R\}/\sigma$
$D_{LL}=(0,L;0,L)$	$\{-2\,\text{Re}[(N_0+N_2)N_1^*]\sin\theta_R-(\lvert N_0\rvert^2-\lvert N_2\rvert^2+\lvert U_0\rvert^2-\lvert U_2\rvert^2)\cos\theta_R\}/\sigma$
3. Three-spin measurement	
$H_{SSN}=(S,S;0,N)$	$-2\,\text{Im}[(U_2+U_0)N_1^*]/\sigma$
$H_{LSN}=(L,S;0,N)$	$2\,\text{Im}(U_0N_0^*-U_2N_2^*)/\sigma$
$H_{SLN}=(S,L;0,N)$	$-2\,\text{Im}(N_0U_2^*-N_2U_0^*)/\sigma$
$H_{LLN}=(L,L;0,N)$	$2\,\text{Im}[(U_2+U_0)N_1^*]/\sigma$
$H_{SNS}=(S,N;0,S)$	$\{2\,\text{Im}[(U_2-U_0)N_1^*]\cos\theta_R+2\,\text{Im}(N_0U_2^*+N_2U_0^*)\sin\theta_R\}/\sigma$
$H_{SNL}=(S,N;0,L)$	$\{2\,\text{Im}[(U_2-U_0)N_1^*]\sin\theta_R-2\,\text{Im}(N_0U_2^*+N_2U_0^*)\cos\theta_R\}/\sigma$
$H_{LNS}=(L,N;0,S)$	$\{-2\,\text{Im}[(U_2-U_0)N_1^*]\sin\theta_R+2\,\text{Im}(U_0N_0^*+U_2N_2^*)\cos\theta_R\}/\sigma$
$H_{LNL}=(L,N;0,L)$	$\{2\,\text{Im}[(U_2-U_0)N_1^*]\cos\theta_R+2\,\text{Im}(U_0N_0^*+U_2N_2^*)\sin\theta_R\}/\sigma$
$H_{NSS}=(N,S;0,S)$	$\{2\,\text{Im}[(N_0+N_2)N_1^*]\cos\theta_R-2\,\text{Im}(U_0U_2^*-N_0N_2^*)\sin\theta_R\}/\sigma$
$H_{NSL}=(N,S;0,L)$	$\{2\,\text{Im}[(N_0+N_2)N_1^*]\sin\theta_R+2\,\text{Im}(U_0U_2^*-N_0N_2^*)\cos\theta_R\}/\sigma$
$H_{NLS}=(N,L;0,S)$	$\{-2\,\text{Im}[(N_0+N_2)N_1^*]\sin\theta_R+2\,\text{Im}(U_0U_2^*+N_0N_2^*)\cos\theta_R\}/\sigma$
$H_{NLL}=(N,L;0,L)$	$\{2\,\text{Im}[(N_0+N_2)N_1^*]\cos\theta_R+2\,\text{Im}(U_0U_2^*+N_0N_2^*)\sin\theta_R\}/\sigma$

TABLE I. (*Continued*).

Observables $(B,T;S,R)$	(b) Helicity amplitudes
(Single scattering)	
σ^{tot}	$(2\pi/k)\text{Im}[\phi_1(0)+\phi_3(0)]$
$\Delta\sigma_L^{\text{tot}}$	$(4\pi/k)\text{Im}[\phi_1(0)-\phi_3(0)]$
$\Delta\sigma_T^{\text{tot}}$	$-(4\pi/k)\text{Im}\phi_2(0)$
$\sigma=(0,0;0,0)$	$\frac{1}{2}(\lvert\phi_1\rvert^2+\lvert\phi_2\rvert^2+\lvert\phi_3\rvert^2+\lvert\phi_4\rvert^2+4\lvert\phi_5\rvert^2)$
$P=(0,N;0,0)$	$\text{Im}[(\phi_1+\phi_2+\phi_3-\phi_4)^*\phi_5]/\sigma$
$C_{NN}=(N,N;0,0)$	$\text{Re}[(\phi_1^*\phi_2-\phi_3^*\phi_4)+2\lvert\phi_5\rvert^2]/\sigma$
$C_{SS}=(S,S;0,0)$	$\text{Re}(\phi_1^*\phi_2+\phi_3^*\phi_4)/\sigma$
$C_{SL}=(S,L;0,0)$	$\text{Re}[(\phi_1+\phi_2-\phi_3+\phi_4)^*\phi_5]/\sigma$
$C_{LL}=(L,L;0,0)$	$\frac{1}{2}[-\lvert\phi_1\rvert^2-\lvert\phi_2\rvert^2+\lvert\phi_3\rvert^2+\lvert\phi_4\rvert^2]/\sigma$
Note: $d\sigma/dt=\sigma\pi/k^2$.	
(Double scattering)	
1. K_{jk} measurement	
$K_{NN}=(N,0;0,N)$	$[-\text{Re}(\phi_1^*\phi_4-\phi_2^*\phi_3)+2\lvert\phi_5\rvert^2]/\sigma$
$K_{SS}=(S,0;0,S)$	$\{\sin\theta_R\text{Re}[(\phi_1-\phi_2-\phi_3-\phi_4)^*\phi_5]-\cos\theta_R\text{Re}(\phi_1^*\phi_4+\phi_2^*\phi_3)\}/\sigma$
$K_{LS}=(L,0;0,S)$	$\{-\frac{1}{2}\sin\theta_R[\lvert\phi_1\rvert^2-\lvert\phi_2\rvert^2-\lvert\phi_3\rvert^2+\lvert\phi_4\rvert^2]+\cos\theta_R\text{Re}[(\phi_1-\phi_2-\phi_3-\phi_4)^*\phi_5]\}/\sigma$
$K_{LL}=(L,0;0,L)$	$\{\sin\theta_R\text{Re}[(\phi_1-\phi_2-\phi_3-\phi_4)^*\phi_5]+\frac{1}{2}\cos\theta_R(\lvert\phi_1\rvert^2-\lvert\phi_2\rvert^2-\lvert\phi_3\rvert^2+\lvert\phi_4\rvert^2)\}/\sigma$
2. D_{jk} measurement	
$D_{NN}=(0,N;0,N)$	$[\text{Re}(\phi_1^*\phi_3-\phi_2^*\phi_4)+2\lvert\phi_5\rvert^2]/\sigma$
$D_{SS}=(0,S;0,S)$	$\{-\sin\theta_R\text{Re}[(\phi_1-\phi_2+\phi_3+\phi_4)^*\phi_5]-\cos\theta_R\text{Re}[(\phi_1^*\phi_3+\phi_2^*\phi_4)]\}/\sigma$
$D_{LS}=(0,L;0,S)$	$\{\frac{1}{2}\sin\theta_R[\lvert\phi_1\rvert^2-\lvert\phi_2\rvert^2+\lvert\phi_3\rvert^2-\lvert\phi_4\rvert^2]-\cos\theta_R\text{Re}[(\phi_1-\phi_2+\phi_3+\phi_4)^*\phi_5]\}/\sigma$
$D_{SL}=(0,S;0,L)$	$\{\cos\theta_R\text{Re}[(\phi_1-\phi_2+\phi_3+\phi_4)^*\phi_5]-\sin\theta_R\text{Re}(\phi_1^*\phi_3+\phi_2^*\phi_4)\}/\sigma$
3. Three-spin measurement	
$H_{SNS}=(S,N;0,S)$	$\{-\sin\theta_R\text{Im}(\phi_1^*\phi_2+\phi_3^*\phi_4)+\cos\theta_R\text{Im}[(\phi_1-\phi_2-\phi_3-\phi_4)^*\phi_5]\}/\sigma$
$H_{NSS}=(N,S;0,S)$	$\{\sin\theta_R\text{Im}(\phi_1^*\phi_2-\phi_3^*\phi_4)-\cos\theta_R\text{Im}[(\phi_1-\phi_2+\phi_3+\phi_4)^*\phi_5]\}/\sigma$
$H_{SSN}=(S,S;0,N)$	$\text{Im}[(\phi_1+\phi_2-\phi_3+\phi_4)^*\phi_5]/\sigma$
$H_{LSN}=(L,S;0,N)$	$-\text{Im}(\phi_1^*\phi_3-\phi_2^*\phi_4)/\sigma$
$H_{NLS}=(N,L;0,S)$	$\{\sin\theta_R\text{Im}[(\phi_1-\phi_2+\phi_3+\phi_4)^*\phi_5]-\cos\theta_R\text{Im}(\phi_1^*\phi_4+\phi_2^*\phi_3)\}/\sigma$
$H_{SLN}=(S,L;0,N)$	$\text{Im}(\phi_1^*\phi_4-\phi_2^*\phi_3)/\sigma$
$H_{LNS}=(L,N;0,S)$	$\{-\sin\theta_R\text{Im}[(\phi_1-\phi_2-\phi_3-\phi_4)^*\phi_5]-\cos\theta_R\text{Im}(\phi_1^*\phi_3+\phi_2^*\phi_4)\}/\sigma$
Note: θ_R is the laboratory recoil angle.	

$$
\begin{aligned}
N_0&=\tfrac{1}{2}(\phi_1+\phi_3)\ ,\\
N_1&=\phi_5\ ,\\
N_2&=\tfrac{1}{2}(\phi_4-\phi_2)\ ,\\
U_0&=\tfrac{1}{2}(\phi_1-\phi_3)\ ,\\
U_2&=\tfrac{1}{2}(\phi_2+\phi_4)\ .
\end{aligned}
\tag{2}
$$

The experimental observables expressed in terms of both sets of amplitudes are summarized in Tables I(a) (Refs. 16 and 21) and I(b) (Ref. 22).

III. EXPERIMENTAL PROCEDURES

The measurements were carried out with the same experimental apparatus using two different directions of the beam spin. Together with an S-type polarized target, an N-polarized beam was used for measurement of H_{NSS} and an L-polarized beam for H_{LSN}. The two beam polarizations were alternated during the same running period so that most systematics are similar for the two measurements. An approximately L-type polarized target was used for the measurement of $\tilde{D}_{LS}$ and other parameters. In this case, L-type and S-type beam polarizations were employed. Figure 2 shows one of the experimental setups, consisting of a beam line with a set of spin precessors (not shown), an S-type polarized target, a forward detecting system, and a recoil polarimeter. The other experimental setup is shown in Ref. 12.

A. Polarized proton beam

Polarized protons entered the beam transport system with spin along the vertical axis. For the H_{LSN} measurement it was necessary that the spin direction be along the beam axis at the center of the polarized proton target (PPT). The magnetic field of the PPT magnet was perpendicular to the N-L plane; this caused significant ($\sim 20°$) precession of the polarized beam. Consequently, the spin direction at the entrance of the PPT was oriented so that this additional rotation produced the spin direction required at the center of the target. Analogous situations existed for the H_{NSS} and L-type target measurements. The proper beam spins were obtained with a versatile beam channel which used both solenoid and dipole magnets; the details have been given elsewhere.[23]

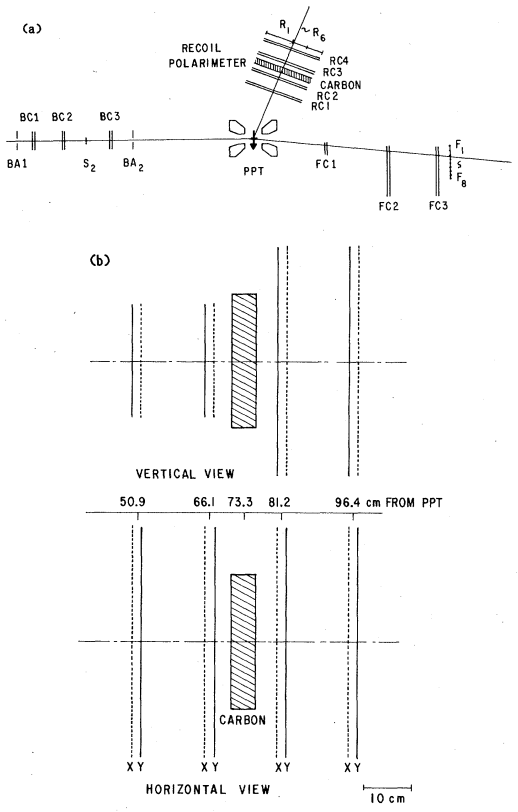

FIG. 2. (a) Experimental layout. (Note that the upstream counters S_0 and S_1 are not shown in the figure.) (b) Configuration of the polarimeter.

For convenience, we define the polarization of the beam as follows:

$$\mathbf{P}_{\text{beam}}=P_B(\alpha_N\hat{\mathbf{N}}+\alpha_L\hat{\mathbf{L}}+\alpha_S\hat{\mathbf{S}})\ , \tag{3}$$

where P_B is the magnitude of the polarization and the α_i are direction cosines of the positive spin vector to unit vectors $\hat{\mathbf{N}}$, $\hat{\mathbf{L}}$, and $\hat{\mathbf{S}}$ as shown in Fig. 1. The values α_N and α_S before the PPT and at the center of the PPT were calculated using the known beam transport parameters and the measured field of the PPT; they are summarized in Table II. The additional deflection of the incident beam in the magnetic field of the PPT was also taken into account in the experimental setup.

The polarity of the beam spin was reversed each spill (every few seconds) to reduce systematic errors. The beam polarization was continuously monitored with a polarimeter whose signals were analyzed by a computer in the ZGS main control room. The intensity was typically 10^6 protons/spill with average polarization of 0.73.

B. Polarized proton target

The polarized proton target consisted of a target cell, a cryostat, and a magnet. The target cell had dimensions of 1.9 cm (W)$\times$2.0 cm (H)$\times$6.5 cm (L) and was filled with 2-mm-diameter beads of ethylene glycol ($HOCH_2CH_2OH$) doped with $K_2Cr_2O_7$. It was cooled by a horizontal ^{3}He refrigerator operating near 0.4 K.

The free protons were dynamically polarized by microwave excitation in the 2.5-T field of the PPT magnet; this consisted of superconducting coils in a Helmholtz-type configuration. The magnetic apertures were cones of 48° along the field axis; recoil protons emerged through one of these. There were equatorial apertures of 21° for the passage of the beam and scattered protons. For the L-target measurements, the beam and scattered protons passed through one of the 48° cones and the recoil protons through the equatorial aperture. In this case there was a restriction to the angular coverage at large $|t|$ caused by the limited recoil aperture.

For the discussion of Sec. IV it is convenient to express the target polarization as

$$\mathbf{P}_{\text{target}}=P_T(\beta_N\hat{\mathbf{N}}+\beta_L\hat{\mathbf{L}}+\beta_S\hat{\mathbf{S}})\ , \tag{4}$$

where the definition of P_T and the β_i are analogous to those for the beam. For the H_{NSS} and H_{LSN} measurements the target was oriented so that β_S was equal to 1.0, while β_N and β_L were equal to zero (see Table III). The magnetic field was oriented at 18° to the beam for the $\tilde{D}_{LS}$

TABLE II. Spin direction of the beam. The beam spin components for Eq. (3) are given below, far from the polarized target, and at the center of the S target. The components for the L target at the target center are given for two scattering angles.

	(S target)			
	N-spin beam		L-spin beam	
Component	Initial	At PPT	Initial	At PPT
α_N	0.939±0.021	$1.000^{+0.000}_{-0.002}$	0.344±0.057	0.020±0.06
α_L	−0.344±0.057	−0.020±0.06	0.939±0.021	$1.000^{+0.000}_{-0.002}$
α_S	0.0±0.06	0.0±0.06	0.0±0.06	0.0±0.06

	(L target)			
	S-spin beam		L-spin beam	
Component	$\|t\|=0.27$	0.66	0.27	0.66 GeV$^2/c^2$
α_N	−0.18±0.06	0.05±0.06	−0.010±0.06	−0.010±0.06
α_L	−0.03±0.06	−0.03±0.06	$-1.000^{+0.002}_{-0.000}$	$-1.000^{+0.002}_{-0.000}$
α_S	0.983±0.011	0.998±0.002	0.01±0.06	0.01±0.06

TABLE III. Spin direction of the target. The target spin components for Eq. (4) are given below for the two target configurations of this experiment. The effects of the rotation of the scattering plane and the detector acceptances have been included.

	(S target)	
β_S	$1.000\,00^{+0}_{-4\times10^{-5}}$	
β_L	$0.00^{+0.01}_{-0}$	
β_N	$0.00^{+0.01}_{-0}$	
	(L target)	
	$\lvert t \rvert = 0.27$	0.66 GeV$^2/c^2$
β_S	0.273±0.008	0.300±0.008
β_L	0.951±0.003	0.951±0.003
β_N	−0.147±0.008	−0.077±0.008

measurements in order to be able to detect both the forward and recoil protons. For the L target, the mean scattering plane was also rotated by the target magnetic field. This affects the β's as shown in Table III. For the S target, the detector placement compensated for the change in the scattering plane. The target polarization was monitored by a NMR system with a pickup coil wound around the target cell. The NMR signals were read in and analyzed continuously by a PDP-11/20 computer. The polarity of the PPT was reversed at approximately 2-h intervals. The average polarization during the experiments was about 0.80.

C. Trigger counters and chambers

The experimental arrangement for the H_{LSN} and H_{NSS} measurements is shown in Fig. 2(a). The beam was defined by scintillation counters S_0 (placed far upstream of the PPT), S_1, and S_2. Beam halo was rejected by BA_1; particles not going through the PPT were rejected by BA_2. Scattered and recoil particles were identified by hodoscopes F_1 through F_8, and R_1 through R_6, respectively. Unscattered beam particles were vetoed. There were three pairs of multiwire proportional chambers (MWPC's) with X and Y planes both upstream of the PPT and in the forward arm for tracking beam and scattered particles.

The recoil particle was detected by a recoil polarimeter which consisted of four pairs of MWPC's and a carbon plate of thickness 5.08 cm that served as scatterer. Each pair of chambers had both X and Y planes with wire spacing of 2 mm. The two pairs of chambers before the carbon had an effective area of 51.2×25.6 cm^2 and the two pairs behind had an effective area of 51.2×51.2 cm^2. The polarimeter is shown schematically in Fig. 2(b). The polarimeter was oriented so that its normal made an angle of 67.06° and 71.25° (for S and L targets, respectively) with respect to the beam axis. The alignment of the polarimeter chambers was checked and calibrated using straight-through data with no PPT magnetic field and no carbon scatterer.

D. Trigger and data acquisition

Events were triggered by $(S_0\cdot S_1\cdot S_2\cdot R_i\cdot F_i\cdot\overline{BA}_i\cdot\text{FEF})$, where FEF was the logic signal from a hard-wired fast-event filter. Output from the polarimeter chambers was supplied to this circuit which calculated the difference between the slope of tracks before and after the carbon scatterer. If the difference was larger than the preset value, the FEF would output an OK signal. Most unscattered events were rejected with this circuit, saving both tapes and computer time which would otherwise be used for analysis. The accepted data were read onto tape through CAMAC using an EMI 6050 computer.

IV. DATA ANALYSIS

A. Data reduction

The data (a total of 38×10^6 events) were analyzed in three stages: (a) filter, (b) analysis, and (c) polarimeter analysis. In the "filter" stage, only those events having enough chamber information for track reconstruction were transmitted to the next stage; the transmission efficiency was about 50%.

In the "analysis" stage, kinematical values were calculated for the first scattering, i.e., scattering at the PPT. In doing this it was necessary that corrections be made for the effects of the PPT magnetic field. The corrections were evaluated by generating large numbers of events with random scattering angle (θ,ϕ) and interaction point within the PPT. For each event the energy losses in the PPT were calculated and the particles tracked through the magnetic field to the chamber planes. The simulated events were fitted to obtain a correlation matrix among the coordinates of the interaction point, the scattering angles (θ,ϕ), and wire numbers in the chambers.

Cuts were made to the data for those events with interaction points outside the target, or too large distance between forward and recoil tracks, etc. However, no cut was made here for either the angle-angle correlation or coplanarity. The distribution of the interaction points at the target is shown in Fig. 3(a). The distribution in coplanarity angle is shown in Fig. 3(b); the coplanar peak is clearly resolved above the noncoplanar background. Approximately 70% of the events survived for stage three analysis.

The final stage of analysis involved the second scattering at the recoil polarimeter. The MWPC's provided two sets of hit points both before and after the carbon scatterer so that the corresponding angles θ_c and ϕ_c could be calculated. The definition of these angles is illustrated in Fig. 4. The laboratory coordinates X,Y,Z are defined with Z along the incident beam direction, X in the horizontal plane, and Y upward. The new Z axis (Z') at the second scattering is along the direction of the recoil proton incident on the carbon plate. The corresponding Y axis (Y') lies in the Y-Z' plane; the new X axis (X') is given by $Y'\times Z'$. The scattering angles θ_c and ϕ_c in the carbon plate are measured with respect to the primed axes. Those events which did not have full acceptance in the last chamber, or events with too large distance between tracks before and after the carbon plate, were reject-

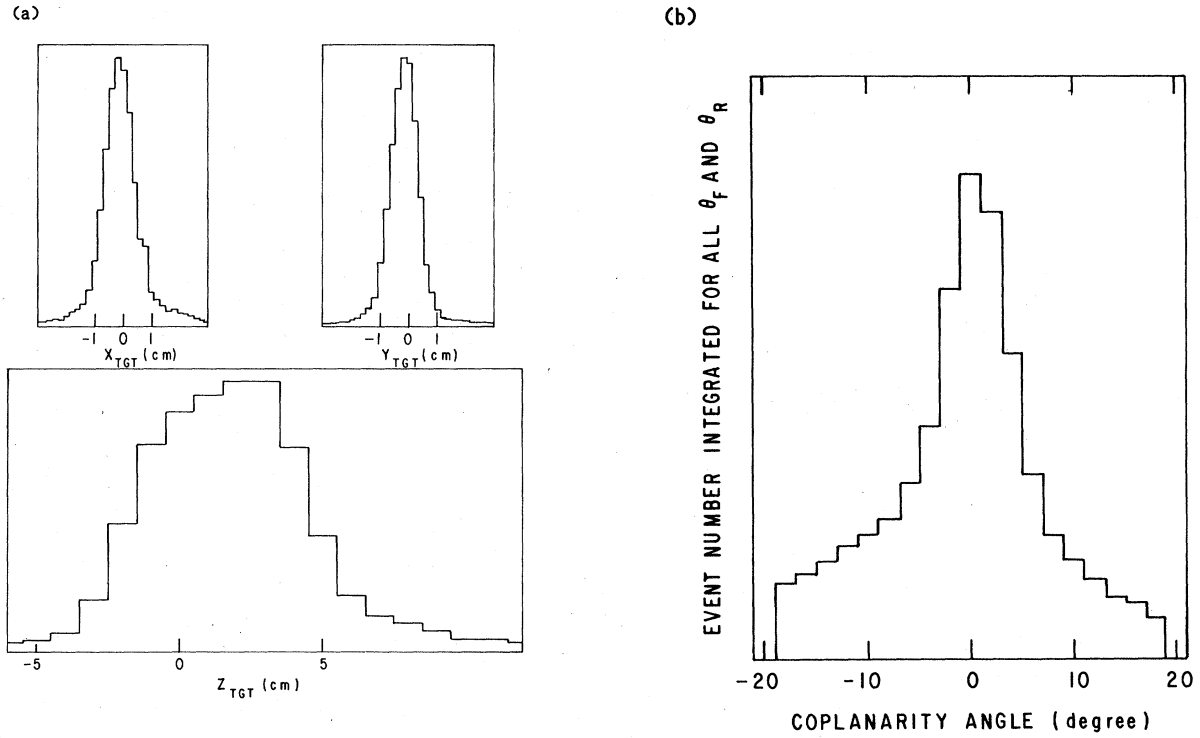

FIG. 3. (a) Distribution of the interaction point at the PPT calculated from the forward and recoil trajectories. (b) Distribution of the coplanarity angle between scattered and recoil particles.

ed. The scattering angle θ_c was limited to the region 6° to 16° in order to be able to compare to the analyzing power of the polarimeter, A_{pC}, as measured in our previous experiment.[1] Even with the fast event filter, only about 5% of the events survived these cuts to be identified as good events. The typical histograms of the scattered-recoil correlation for both coplanar and noncoplanar events from the first scattering are shown in Fig. 5. The arrows

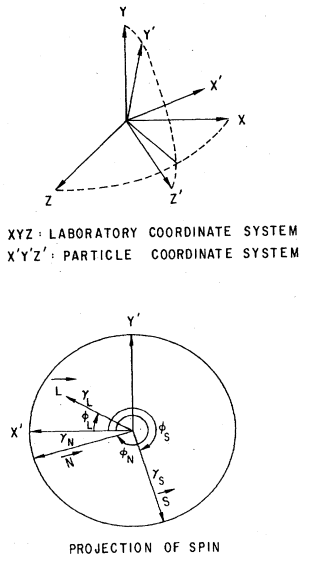

FIG. 4. Definition of the coordinate system used in the polarimeter analysis. The laboratory coordinates have Z along the incident beam direction and Y up. The X', Y', Z' coordinates correspond to the recoil particle as described in the text. The components of the recoil particle spin in the $X'Y'$ plane (perpendicular to its direction of motion) are given in terms of γ and ϕ as shown.

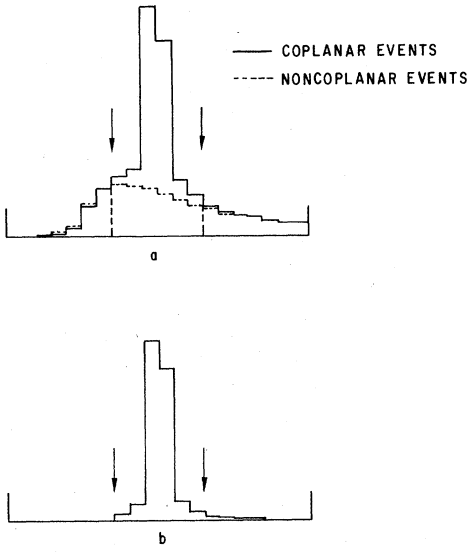

FIG. 5. Typical distribution of the product $\tan\theta_{scatt}\tan\theta_{recoil}$. This peaks near $4M_p^2/s$ where M_p is the proton mass and s is the square of the total energy. (a) Both coplanar and noncoplanar events. (b) The distribution after the subtraction of noncoplanar events from coplanar ones. Arrows show the position of the cuts.

in the histogram are the positions of the cuts. To estimate contributions from inelastic and quasifree scattering from the carbon in the PPT the noncoplanar events were normalized to the number of coplanar events outside the cut lines. Then at the recoil polarimeter the azimuthal distribution of the normalized noncoplanar events was subtracted from that of the coplanar events.

The superconducting magnet of the PPT, shown in Fig. 2, had a strength of 2.5 T in the target region. It was designed with no return yoke to provide maximum acceptance in the L and S configurations; the consequence, however, is a large fringe field outside the magnet. The magnetic field remained strong (0.6—0.2 T) in the region of the polarimeter whose center was about 70 cm from the PPT. Since the recoil protons were of low momentum (0.4—1.2 GeV/c) it was important to correct for precession of their spins in the fringe field.

In the analysis of the double-scattering events it is necessary to know the orientation of the spin of the recoil proton immediately before the second scattering in the polarimeter. For the azimuthal asymmetry the relevant part is the projection γ and the azimuthal angle ϕ_c in the X'-Y' plane in Fig. 4. We have calculated these values as a function of $|t|$ for recoils initially (i.e., at the PPT) polarized along the L, N, and S directions. The results are shown in Fig. 6(a) for the S-target measurements and Fig. 6(b) for the L-target measurements; angles and energy losses were calculated in the approximation that all interactions occurred in the center of the PPT.

After scattering by the carbon in the polarimeter the number of events in the ith azimuthal bin can be written as

$$N^{\pm\pm}(\phi_i)=\eta(\phi_i)I_0[1+a_0^{\pm\pm}-a_N^{\pm\pm}\sin(\phi_i-\phi_N) -a_L^{\pm\pm}\sin(\phi_i-\phi_L) -a_S^{\pm\pm}\sin(\phi_i-\phi_S)]\,, \quad (5)$$

where the superscripts indicate directions of beam and target polarizations, and the coefficients a_j may be expressed in terms of P_B, P_T, and the spin parameters. The distortion function, $\eta(\phi_i)$, takes into account the effect of the magnetic field on recoil protons, binning of events in the chamber, etc. The subscripts N, L, and S denote the components of recoil spin at the PPT. The detailed expressions for a_j and the experimental determination of the distortion function, $\eta(\phi_i)$, are given in the Appendix.

The data were taken for four combinations of beam and target polarizations. The azimuthal distributions were obtained for each t bin used in the first scattering. The angular range of 360° was divided into 24 bins, −7.5° to

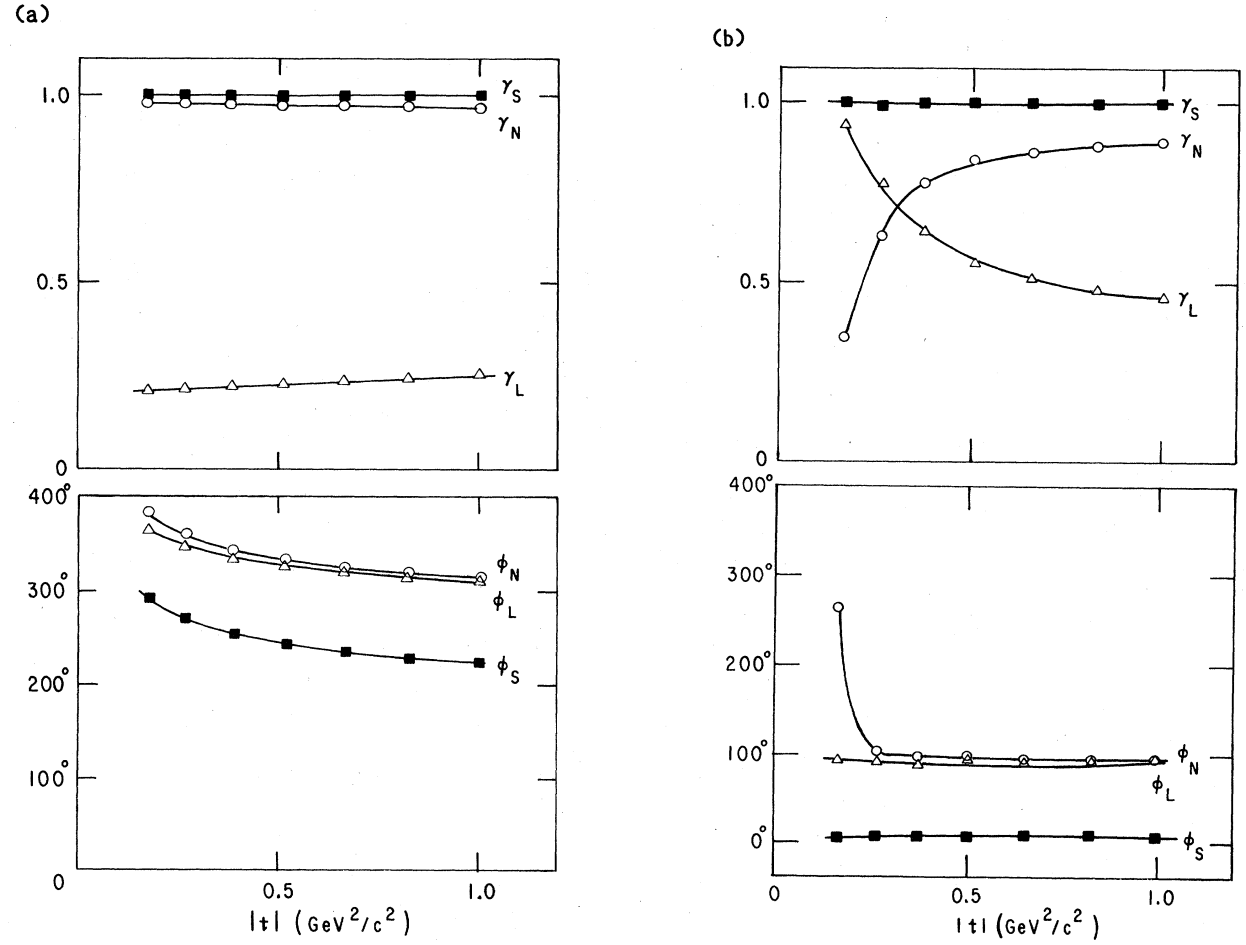

FIG. 6. Calculated values of γ's and ϕ's for various four-momentum-transfer-squared $|t|$. (a) S target, (b) L target.

7.5°, 7.5° to 22.5°, etc. The raw azimuthal distributions were next corrected for beam and target polarizations, and the distortion functions. The distributions were then normalized and constant terms subtracted; details are again described in the Appendix. The resulting distributions can now be expressed in terms of physical parameters of interest. For example, with a pure N beam and S target ($\alpha_N=1.00$, $\beta_S=1.00$) the distributions are

$$\begin{aligned} n^{(1)}(\phi)&=A_{pC}\gamma_N P\sin(\phi-\phi_N)\ , \\ n^{(2)}(\phi)&=A_{pC}\gamma_N K_{NN}\sin(\phi-\phi_N)\ , \\ n^{(3)}(\phi)&=A_{pC}[\gamma_L D_{SL}\sin(\phi-\phi_L)+\gamma_S D_{SS}\sin(\phi-\phi_S)]\ , \\ n^{(4)}(\phi)&=A_{pC}[\gamma_L H_{NSL}\sin(\phi-\phi_L)+\gamma_S H_{NSS}\sin(\phi-\phi_S)]\ , \end{aligned} \tag{6}$$

where the definition of $n^{(i)}(\phi)$ is given in Eq. (A13) of the Appendix. In the principle there are additional terms due to imperfect alignment of the initial spin states; however, with the high degree of spin alignment achieved in the present experiment (see Tables II and III), their contributions are usually negligible. It is now possible to fit the experimental azimuthal distributions, $n^{(k)}(\phi_i)$, for each t bin to an expression of the above form with given values of the γ and ϕ parameters; further details appear in the Appendix (see also Table IV). Note that in Eq. (6), ϕ_S and ϕ_L differ by approximately 90°, so that pure D_{SS} and H_{NSS} can be derived.

The results obtained are shown in Fig. 7 and listed in Table V.

B. Discussion of systematic errors

The distortion function $\eta(\phi)$ was introduced to take into account the effects of the magnetic field on recoil protons. However, there are other effects which could in-

TABLE IV. Coefficients of spin parameters. The asterisk denotes the large components. The polarization P was used with existing data to determine the distortions due to the target magnetic field (see the text).

	$-t$ [GeV/c)^2]	0.27	0.38	0.51	0.66	0.83	1.00	Error
(i)	L beam, S target							
P^*		0.98	0.98	0.97	0.97	0.97	0.97	0.02
K_{LS}^*		0.998	0.999	0.999	1.000	1.000	1.000	0.004
$\tilde{K}_{LL}$	K_{LL}	0.24	0.23	0.24	0.24	0.25	0.26	0.08
	K_{NN}	0.02	0.02	0.02	0.02	0.02	0.02	0.06
D_{SS}^*		0.998	0.999	0.999	1.000	1.000	1.000	0.004
D_{SL}		0.24	0.23	0.24	0.24	0.25	0.26	0.08
H_{LSN}^*		0.98	0.97	0.97	0.97	0.97	0.97	0.02
H_{NSS}		0.02	0.02	0.02	0.02	0.02	0.02	0.06
(ii)	N beam, S target							
P^*		0.98	0.98	0.97	0.97	0.97	0.97	0.02
K_{NN}^*		0.98	0.97	0.97	0.97	0.97	0.97	0.02
K_{LS}		0.02	0.02	0.02	0.02	0.02	0.02	0.06
D_{SS}^*		0.998	0.999	0.999	1.000	1.000	1.000	0.004
D_{SL}		0.24	0.23	0.24	0.24	0.25	0.26	0.08
H_{NSS}^*		0.998	0.999	0.999	1.000	1.000	1.000	0.004
$\tilde{H}_{NSL}$	H_{NSL}	0.24	0.23	0.24	0.24	0.25	0.26	0.08
	H_{LSN}	−0.02	−0.02	−0.02	−0.02	−0.02	−0.02	0.06
(iii)	L beam, L target							
P^*		0.63	0.77	0.83	0.86	...	...	0.05
$\tilde{K}_{LS}^*$	K_{LS}	0.996	0.999	1.000	1.000	...	...	0.002
	K_{SS}	−0.01	−0.01	−0.01	−0.01	...	...	0.06
$\tilde{K}_{LL}^*$	K_{LL}	0.78	0.64	0.56	0.51	...	...	0.06
	K_{NN}	0.01	0.01	0.01	0.01	...	...	0.08
$\tilde{D}_{LS}^*$	D_{LS}	0.947	0.950	0.951	0.951	...	...	0.004
	D_{SS}	0.272	0.289	0.296	0.300	...	...	0.008
$\tilde{D}_{LL}^*$	D_{LL}	0.74	0.60	0.53	0.49	...	...	0.06
	D_{SL}	0.21	0.18	0.17	0.15	...	...	0.06
	D_{NN}	−0.09	−0.09	−0.08	−0.07	...	...	0.08
$\tilde{H}_{LNS}$	H_{LNS}	0.15	0.11	0.09	0.08	...	...	0.01
	H_{NLS}	−0.01	−0.01	−0.01	−0.01	...	...	0.06
$\tilde{H}_{LLN}^*$	H_{LLN}	0.60	0.74	0.79	0.82	...	...	0.05
	H_{LSN}	0.17	0.22	0.24	0.26	...	...	0.05
	H_{LNL}	−0.12	−0.07	−0.05	−0.04	...	...	0.06
	H_{NLL}	0.01	0.01	0.01	0.01	...	...	0.08
	H_{SLN}	0.00	0.00	−0.01	−0.01	...	...	0.08

TABLE IV. (*Continued*).

	$-t$ [GeV/c)^2]	0.27	0.38	0.51	0.66	0.83	1.00	Error
(iv)	S beam, L target							
P^*		0.63	0.77	0.83	0.86	. . .	. . .	0.05
$\tilde{K}^*_{SS}$	K_{SS}	0.979	0.997	1.000	0.998	. . .	. . .	0.004
	K_{LS}	−0.03	−0.03	−0.03	−0.03	. . .	. . .	0.06
$\tilde{K}^*_{SL}$	K_{SL}	0.77	0.64	0.56	0.51	. . .	. . .	0.06
	K_{NN}	−0.11	−0.05	0.01	0.04	. . .	. . .	0.08
	K_{LL}	−0.02	−0.02	−0.02	−0.01	. . .	. . .	0.08
$\tilde{D}^*_{LS}$	D_{LS}	0.947	0.950	0.951	0.951	. . .	. . .	0.004
	D_{SS}	0.272	0.289	0.296	0.300	. . .	. . .	0.008
$\tilde{D}^*_{LL}$	D_{LL}	0.74	0.60	0.53	0.49	. . .	. . .	0.06
	D_{SL}	0.21	0.18	0.17	0.15	. . .	. . .	0.06
	D_{NN}	−0.09	−0.09	−0.08	−0.07	. . .	. . .	0.08
$\tilde{H}_{SNS}$	H_{SNS}	0.14	0.11	0.09	0.08	. . .	. . .	0.02
	H_{NLS}	0.17	0.06	−0.01	−0.05	. . .	. . .	0.06
	H_{NSS}	0.05	0.02	0.00	−0.02	. . .	. . .	0.06
$\tilde{H}^*_{SLN}$	H_{SLN}	0.59	0.73	0.79	0.81	. . .	. . .	0.06
	H_{SSN}	0.17	0.22	0.24	0.26	. . .	. . .	0.06
	H_{SNL}	−0.11	−0.07	−0.05	−0.04	. . .	. . .	0.06
	H_{NLL}	−0.14	−0.04	0.00	0.03	. . .	. . .	0.08
	H_{LLN}	−0.02	−0.02	−0.02	−0.02	. . .	. . .	0.08
	H_{LSN}	−0.01	−0.01	−0.01	−0.01	. . .	. . .	0.08
	H_{NSL}	−0.04	−0.01	0.00	0.01	. . .	. . .	0.08

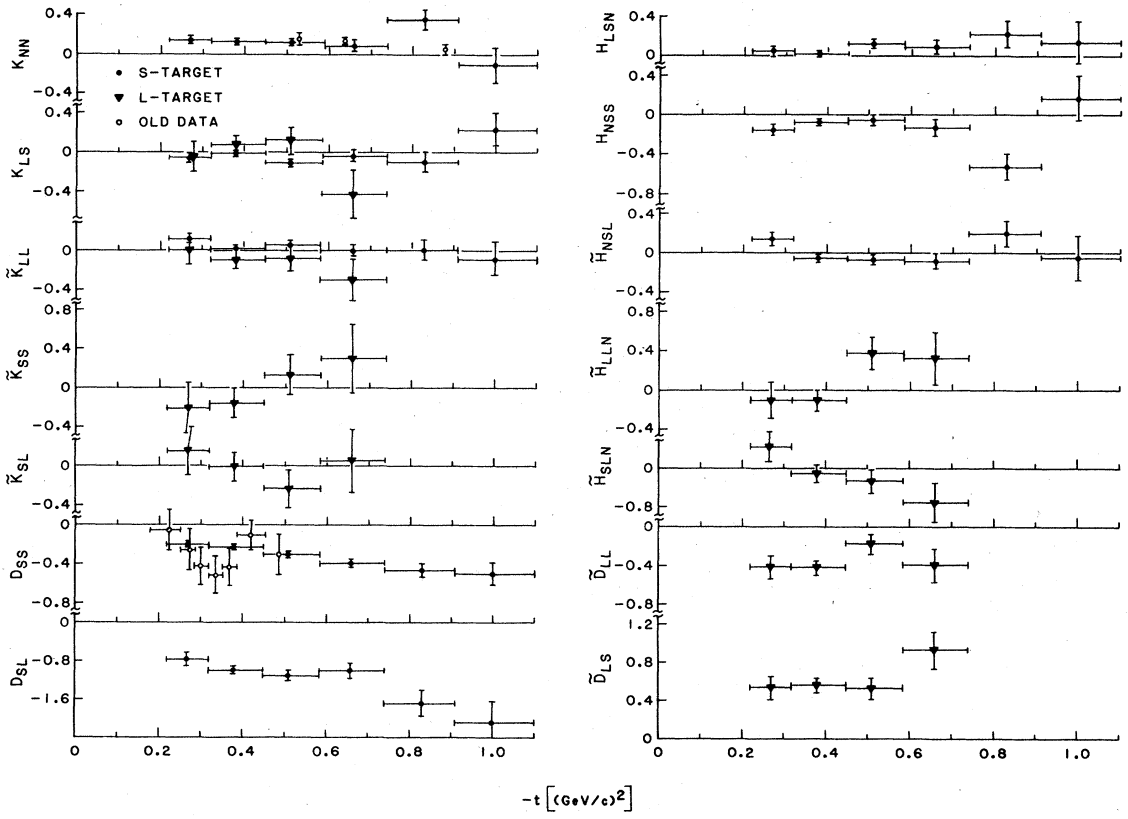

FIG. 7. Measured spin observables. Closed circles and triangles are the present data, and open ones (Refs. 2 and 5) are existing data referred to in Sec. IV C.

TABLE V. Measured observables with S and L targets. Numerical values for the pure spin parameters, such as K_{LS}, D_{SL}, H_{NSS}, have been corrected by the components in Table IV. No corrections have been applied for the mixed spin parameters, such as $\tilde{K}_{LL}$, $\tilde{H}_{LLN}$, or $\tilde{H}_{SNS}$. The errors quoted are statistical only. Estimated systematic uncertainties are given in Table VI.

(i) L beam, S target

$\bar{t}$ [(GeV/c)^2]	K_{LS}	$\tilde{K}_{LL}$	D_{SS}	D_{SL}	H_{LSN}
−0.27	−0.056±0.043	0.120±0.048	−0.273±0.043	−0.70±0.21	0.039±0.056
−0.38	−0.012±0.024	0.020±0.024	−0.213±0.024	−1.05±0.11	0.023±0.031
−0.51	−0.110±0.035	0.062±0.036	−0.284±0.035	−1.10±0.15	0.124±0.045
−0.66	−0.042±0.056	0.000±0.056	−0.317±0.055	−1.43±0.23	0.091±0.073
−0.83	−0.102±0.100	0.006±0.103	−0.490±0.093	−1.14±0.38	0.223±0.131
−1.00	0.233±0.163	−0.082±0.170	−0.507±0.161	−1.83±0.63	0.139±0.216

(ii) N beam, S target

$\bar{t}$ [(GeV/c)^2]	K_{NN}	D_{SS}	D_{SL}	H_{NSS}	$\tilde{H}_{NSL}$
−0.27	0.134±0.045	−0.141±0.039	−0.83±0.19	−0.155±0.058	0.132±0.064
−0.38	0.126±0.025	−0.240±0.023	−0.94±0.10	−0.078±0.033	−0.064±0.034
−0.51	0.114±0.037	−0.307±0.033	−1.09±0.14	−0.054±0.054	−0.072±0.048
−0.66	0.079±0.061	−0.454±0.052	−0.61±0.22	−0.134±0.075	−0.087±0.076
−0.83	0.349±0.103	−0.426±0.093	−2.20±0.38	−0.530±0.127	0.188±0.130
−1.00	−0.113±0.179	−0.488±0.154	−2.34±0.61	0.169±0.219	−0.053±0.224

(iii) L beam, L target

$\bar{t}$ [(GeV/c)^2]	$\tilde{K}_{LS}$	$\tilde{K}_{LL}$	$\tilde{D}_{LS}$	$\tilde{D}_{LL}$	$\tilde{H}_{LNS}$	$\tilde{H}_{LLN}$
−0.27	−0.050±0.149	0.008±0.147	0.583±0.136	−0.529±0.134	0.238±0.186	−0.110±0.184
−0.38	0.070±0.093	−0.096±0.087	0.530±0.084	−0.419±0.079	−0.179±0.116	−0.111±0.108
−0.51	0.117±0.135	−0.081±0.130	0.521±0.123	−0.210±0.119	0.227±0.168	0.373±0.163
−0.66	−0.426±0.244	−0.294±0.215	0.873±0.022	−0.374±0.196	−0.654±0.304	0.317±0.269

(iv) S beam, L target

$\bar{t}$ [(GeV/c)^2]	$\tilde{K}_{SS}$	$\tilde{K}_{SL}$	$\tilde{D}_{LS}$	$\tilde{D}_{LL}$	$\tilde{H}_{SNS}$	$\tilde{H}_{SLN}$
−0.27	−0.207±0.256	0.159±0.246	0.287±0.234	−0.017±0.223	0.564±0.320	0.428±0.306
−0.38	−0.155±0.151	−0.013±0.142	0.616±0.137	−0.341±0.130	0.252±0.188	−0.120±0.178
−0.51	0.133±0.199	−0.232±0.191	0.462±0.182	−0.131±0.174	0.103±0.249	−0.279±0.238
−0.66	0.305±0.348	0.059±0.324	0.878±0.318	−0.402±0.296	−0.292±0.435	−0.712±0.405

(v) Averages

$\bar{t}$ [(GeV/c)^2]	D_{SS}	D_{SL}	$\tilde{D}_{LS}$	$\tilde{D}_{LL}$
−0.27	−0.203±0.029	−0.76±0.14	0.533±0.120	−0.417±0.116
−0.38	−0.226±0.017	−0.99±0.07	0.559±0.072	−0.425±0.067
−0.51	−0.296±0.024	−1.10±0.10	0.526±0.102	−0.185±0.099
−0.66	−0.389±0.038	−1.00±0.16	0.927±0.188	−0.396±0.172
−0.83	−0.459±0.066	−1.67±0.27		
−1.00	−0.496±0.112	−2.09±0.44		

fluence the empirical evaluation of this function through $X_0(\phi)$ as described in the Appendix. For example, some structure is introduced if the relative normalization of the beam and target polarizations is not correct. The magnitude of such an effect depends upon some spin parameter such as K_{NN}, etc.

To check for such effects two methods of normalization were tried. The first normalization used the number of protons in the beam and the second used the number of unpolarized background events from the carbon. The latter was used only for the L beam because an N beam can produce an asymmetry on an unpolarized target. No significant difference was observed. The difference between the results obtained with these two normalizations was about an order of magnitude smaller than the statistical error quoted in Table V.

As another test of the stability of our results we varied the value of the analyzing power (P) for p-p scattering in obtaining $\eta(\phi)$ and spin parameters from the azimuthal distributions. Differences due to variations in P of 0.01 to 0.02 were comparable with those described above. An internal check on the consistency of our normalizations is provided by comparing the values of D_{SS} and D_{SL} obtained with the L and N beams and of $\tilde{D}_{LS}$ and $\tilde{D}_{LL}$ with L and S beams. The values are listed in Table V and are consistent within errors.

A Monte Carlo simulation provided a final check of the effect of the magnetic field. The effects of multiple scattering in the PPT and deflection in the fringe field over the region of the polarimeter were introduced. The events generated were analyzed by the same program used for the experimental data. The azimuthal distributions of these simulated events were compared with the observed distributions; the result is shown in Fig. 8. The fair agreement provides support for the assumption that the structure in the ϕ_c distribution is largely due to the magnetic field. More refined treatment of multiple scattering, energy loss, etc., would presumably provide even better agreement.

The normalization constants for double- and triple-spin parameters are given by

$$f_K = A_{pC} P_B \alpha\gamma \quad \text{for } (*,0;0,*)\,,$$
$$f_D = A_{pC} P_T \beta\gamma \quad \text{for } (0,*;0,*)\,, \tag{7}$$

and

$$f_H = A_{pC} P_B P_T \alpha\beta\gamma \quad \text{for } (*,*;0,*)\,,$$

where A_{pC} is the analyzing power for the p-C scattering, taken from Ref. 24. The normalization errors for absolute beam and target polarizations are estimated to be about $\pm 5\%$. The direction of beam and target spins were known to accuracies of $\pm 3.5°$ and $\pm 0.5°$, respectively. These errors are listed in Tables II and III; they are negligible for the coefficients of the large components in Table IV (also see Appendix). The sources of the error in γ and ϕ_c result from accuracy of knowledge of the magnetic field and approximation in the calculation itself. A summary of the systematic errors due to α, β and γ is presented in Table VI. The values of A_{pC} and their estimated systematic uncertainties are given in Table VII.

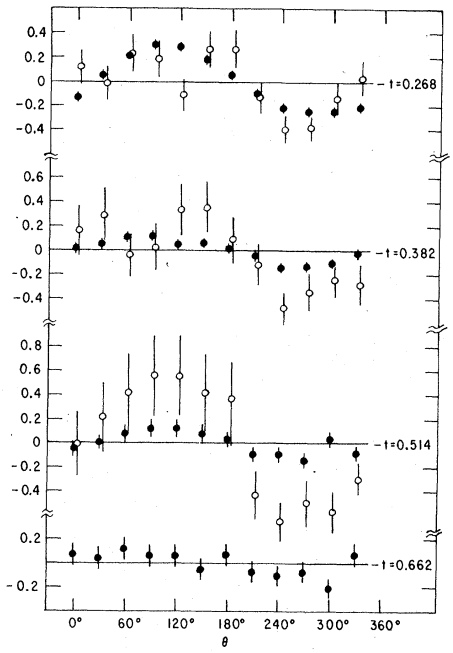

Fig. 8. Comparison of the quantity $\eta(\phi)-1$, where $\eta(\phi)$ is the distortion function for the experimental data and the crude Monte Carlo calculation described in the text. The experimental results have been omitted at $-t=0.66$ (GeV/c)^2 because of the large statistical errors. Open circles, experimental data; closed circles, Monte Carlo.

TABLE VI. Estimated systematic uncertainties (excluding carbon analyzing power). Fractional errors on the experimental measurements are estimated below. Contributions are from uncertainties in the beam, target, and recoil spin projections, α,β,γ, from Table IV and from the beam and target polarization, $P_B P_T$. Note especially the large systematic uncertainties for the S-target parameters $\tilde{K}_{LL}$, D_{SL}, and $\tilde{H}_{NSL}$.

Spin parameter	α,β,γ	P_B,P_T	Total
K_{LS}	0.004	0.050	0.050
$\tilde{K}_{LL}$	0.33	0.050	0.33
D_{SS}	0.004	0.050	0.050
D_{SL}	0.33	0.050	0.33
H_{LSN}	0.021	0.071	0.074
K_{NN}	0.021	0.050	0.054
H_{NSS}	0.004	0.071	0.071
$\tilde{H}_{NSL}$	0.33	0.071	0.34
$\tilde{K}_{LS}$	0.002	0.050	0.050
$\tilde{K}_{LL}$	0.10	0.050	0.11
$\tilde{D}_{LS}$	0.004	0.050	0.050
$\tilde{D}_{LL}$	0.10	0.050	0.11
$\tilde{H}_{LLN}$	0.07	0.071	0.10
$\tilde{K}_{SS}$	0.004	0.050	0.050
$\tilde{K}_{SL}$	0.10	0.050	0.11
$\tilde{H}_{SLN}$	0.08	0.071	0.11

TABLE VII. Estimated values of A_{pC} and systematic uncertainties. The estimated values of the carbon analyzing power, A_{pC}, were taken from Fig. 12 and Ref. 24. Previously measured values (Ref. 1) with a thinner carbon scatterer at small t are also included. The quoted uncertainties are estimated systematic errors for this experiment and statistical errors for the data from Ref. 1.

$-t$ [(GeV/c)^2]	A_{pC} (this expt)	A_{pC} (Ref. 1)
0.27	0.15±0.08	0.31±0.04
0.38	0.49±0.05	0.59±0.06
0.51	0.51±0.05	0.51±0.07
0.66	0.43±0.04	0.43±0.07
0.83	0.33±0.03	0.37±0.10
1.00	0.27±0.03	0.29±0.12

The errors in normalization may be estimated by combining those errors for the large component in quadrature. We obtain

$$\frac{\Delta f_K}{f_K}\sim\frac{\Delta f_D}{f_D}\sim 0.05\ ,\quad \frac{\Delta f_H}{f_H}\sim 0.07\ . \tag{8}$$

No error has been included for the analyzing power of the polarimeter.

There is no observable in the present experiment which provides a useful internal calibration of the polarimeter. In principle, the polarization $(0,0;0,N)$ could provide such a calibration; however, the small azimuthal asymmetry in the second scattering is completely masked by other effects. As an approximation we have used the values of A_{pC} polarization measured in previous experiments.[24] Further discussion on A_{pC} is given in Sec. IV D.

C. Consistency checks with existing data

There are a number of internal consistency checks which can be applied to the present data to search for possible systematic errors. The first three deal with data whose carbon analyzing powers A_{pC} are all related. Then, there are checks for systematic errors for observables which should vanish. Additional tests which permit comparisons of A_{pC} to other experiments are given in Sec. IV D.

Time-reversal invariance leads to some simple relations in the c.m. frame. Converting the spin directions to the laboratory system leads to the equation[21]

$$(D_{SS}-D_{LL})=\cot\theta_R(D_{LS}+D_{SL})\ , \tag{9}$$

where θ_R is the laboratory recoil angle. This relation can also be derived from the formulas in Table I. Note that the carbon analyzing power A_{pC} cancels in this equation, so this is a test for other types of systematic errors. From Table V, the S-target measurements provide pure values of D_{SS} and D_{SL}. The L-target data give mixtures of D_{LS} and D_{SS} ($\tilde{D}_{LS}$) and of D_{LL}, D_{SL}, and D_{NN} ($\tilde{D}_{LL}$). It was assumed that $D_{NN}=0.95$ over the angular range of this experiment; this is the same assumption made in Ref. 1 to obtain A_{pC}. Derived values of the pure D_{ij} spin parameters and of the two sides of Eq. (9) are given in Table VIII. The results of this test are also plotted as a function of $-t$ in Fig. 9(a). It can be seen that the data are consistent with Eq. (9).

Arguments similar to those above lead to the equation[21]

$$(K_{SS}-K_{LL})=\cot\theta_R(K_{LS}+K_{SL})\ . \tag{10}$$

From Table V, the S-target measurements provide pure values of K_{NN} and K_{LS}, and a mixture of K_{NN} and K_{LL}. The L-target data provide two mixtures of K_{SS} and K_{LS} and two mixtures of K_{NN}, K_{SL}, and K_{LL}. Finally, Ref. 1 provides another mixture of K_{SS}, K_{LS}, K_{SL}, and K_{LL}. From this information, pure K_{ij} spin parameters were derived as well as the quantities $(K_{SS}-K_{LL})$ and $\cot\theta_R$ $(K_{LS}+K_{SL})$. The numerical values are given in Table IX, and the last two quantities are also plotted in Fig. 9(b). Again, the results are consistent with Eq. (10). Other checks of this type, for example,

$$\begin{aligned}(H_{LNL}-H_{SNS})&=\tan\theta_R(H_{LNS}+H_{SNL})\ ,\\ (H_{NLL}-H_{NSS})&=\tan\theta_R(H_{NLS}+H_{NSL})\ ,\end{aligned} \tag{11}$$

could not be made for lack of sufficient data.

Another check of the K_{NN} results can be made by comparison to previous measurements of Fernow *et al.*[2] Near $-t=0.5$ (GeV/c)^2, the earlier data gave K_{NN}

TABLE VIII. Derived values of D_{SS}, D_{LS}, D_{SL}, and D_{LL} from measured spin parameters.

$-\bar{t}$ (GeV^2/c^2)	0.27	0.38	0.51	0.66
D_{SS}	−0.203±0.029	−0.226±0.017	−0.296±0.024	−0.389±0.038
D_{LS}	+0.621±0.125	+0.656±0.076	+0.645±0.107	+1.098±0.198
D_{SL}	−0.765±0.145	−0.987±0.072	−1.10±0.10	−1.00±0.16
D_{LL}	−0.224±0.162	−0.269±0.113	+0.129±0.188	−0.367±0.356
$D_{SL}+D_{LS}$	−0.144±0.191	−0.331±0.105	−0.455±0.147	+0.098±0.255
$(\cot\theta_R)(D_{SL}+D_{LS})$	−0.047 ±0.062	−0.130±0.041	−0.209±0.067	+0.051±0.134
$D_{SS}-D_{LL}$	+0.021±0.164	+0.043±0.114	−0.425±0.189	−0.022±0.358
D_{SR}	−0.790±0.138	−1.002±0.067	−1.123±0.092	−1.066±0.143
D_{Sr}	−0.045±0.053	−0.151±0.031	−0.190±0.047	−0.121±0.081
D_{LR}	−0.020±0.159	−0.010±0.109	+0.386±0.177	+0.185±0.328
D_{Lr}	−0.660±0.129	−0.709±0.082	−0.532±0.124	−1.143±0.241

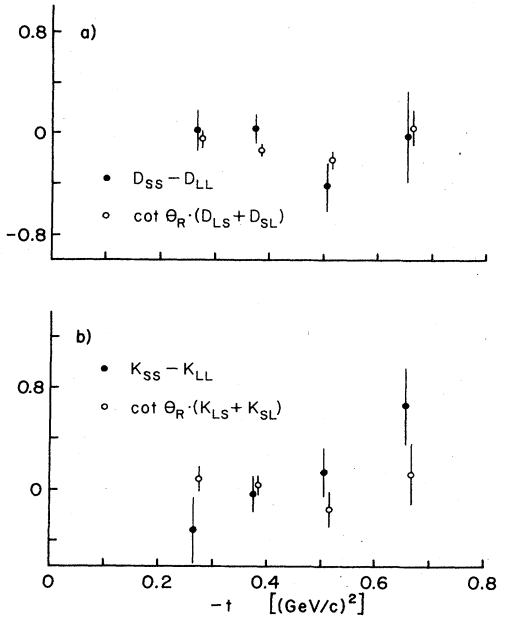

FIG. 9. Tests for consistency of the D_{ij} and K_{ij} data obtained in this experiment. At each t, the two points should be equal.

$=0.14\pm0.08$, whereas Table V gives $K_{NN}=0.114\pm0.037$; see also Fig. 7. This check does not provide a strong test of the value of A_{pC} because the same polarimeter and carbon analyzing power was used to obtain K_{NN} and D_{NN} in Ref. 2. In turn, these values of D_{NN} were used to obtain A_{pC} for the polarimeter in Ref. 1, which are similar to the A_{pC} used in this paper. In summary, there are no indications of sizable systematic errors in the data on the basis of the last three checks.

Another test for systematic errors involves a comparison between D_{SS} data of the Saclay group[5] and the present results; both are shown in Fig. 7. Although the earlier measurements have sizable statistical uncertainty, there is some indication that the present data may be too small in the region $-t\approx0.3$ to 0.4 $(\mathrm{GeV}/c)^2$. Otherwise there is satisfactory agreement.

Finally, parity conservation requires that only spin observables with an even number of L and S subscripts may be different from zero. In a number of measurements performed during these experiments, spin parameters which should nearly vanish were obtained. These include "$\tilde{H}_{LNS}$" with an L beam and L target, and "$\tilde{H}_{SNS}$" with an S beam and L target, for which the coefficients in Table IV are quite small. These results are plotted in Fig. 10 and they are all consistent with zero within statistics, as expected. This test demonstrates that sizable instrumental asymmetries are not present in the data.

D. The carbon analyzing power

It was not possible to obtain an internal calibration of the carbon analyzing power A_{pC} from these data. As a consequence, values from Ref. 24 were used. Some tests are possible to verify that A_{pC} was the same for the S-target and L-target data reported in this paper. Other tests allow cross checks with earlier data. Finally, the value of A_{pC} can be compared to results of our previous measurements.[1]

A test of the consistency of A_{pC} between the S- and L-target data can be performed using the D_{SS}, D_{SL}, $\tilde{D}_{LS}$, and $\tilde{D}_{LL}$ results. In order to satisfy Eq. (9), the ratio of analyzing powers for L- to S-target data must be

$$A_{pC}(L)/A_{pC}(S)=\begin{cases}0.82\pm0.40 & [t=-0.27\ (\mathrm{GeV}/c)^2]\ ,\\ 0.63\pm0.18 & [t=-0.38\ (\mathrm{GeV}/c)^2]\ .\end{cases} \tag{12}$$

Both of these values are consistent with the value 1.00 assumed in this paper.

A different type of test is permitted if it is assumed that the N_0 amplitude is dominant and purely positive imaginary. Then the parameters C_{NN} and K_{NN} can be expressed as follows:

$$C_{NN}\approx 2\,\mathrm{Re}(-N_0N_2^*)/\sigma\approx -2\frac{\mathrm{Im}N_2}{|N_0|}\ ,$$
$$K_{NN}\approx -2\,\mathrm{Re}(N_0N_2^*)/\sigma\approx -2\frac{\mathrm{Im}N_2}{|N_0|}\ . \tag{13}$$

Thus, C_{NN} should be approximately the same as K_{NN}. Another way to show this is to use the expressions in Table I(a):

TABLE IX. Derived values of K_{NN}, K_{SS}, K_{LS}, K_{SL} and K_{LL} from measured spin parameters.

$-\bar{t}$ (GeV$^2/c^2$)	0.27	0.38	0.51	0.66
K_{NN}	0.136±0.043	0.126±0.024	0.118±0.038	0.079±0.062
K_{SS}	−0.085±0.227	−0.042±0.125	0.264±0.152	0.514±0.233
K_{LS}	−0.058±0.041	−0.008±0.023	−0.098±0.030	−0.061±0.054
K_{SL}	0.335±0.283	0.094±0.196	−0.231±0.306	0.303±0.446
K_{LL}	0.234±0.134	−0.008±0.082	0.128±0.135	−0.152±0.206
$K_{SL}+K_{LS}$	0.277±0.285	0.085±0.197	−0.328±0.310	0.243±0.449
$(\cot\theta_R)(K_{LS}+K_{SL})$	0.091±0.093	0.034±0.077	−0.151±0.142	0.128±0.236
$K_{SS}-K_{LL}$	−0.318±0.260	−0.034±0.142	0.136±0.194	0.667±0.304
K_{SR}	0.293±0.256	0.072±0.173	−0.100±0.252	0.508±0.342
K_{Sr}	0.186±0.258	0.073±0.157	−0.336±0.231	−0.315±0.369
K_{LR}	0.203±0.128	−0.011±0.076	+0.076±0.124	−0.163±0.184
K_{Lr}	0.128±0.058	0.005±0.036	0.142±0.061	−0.017±0.108

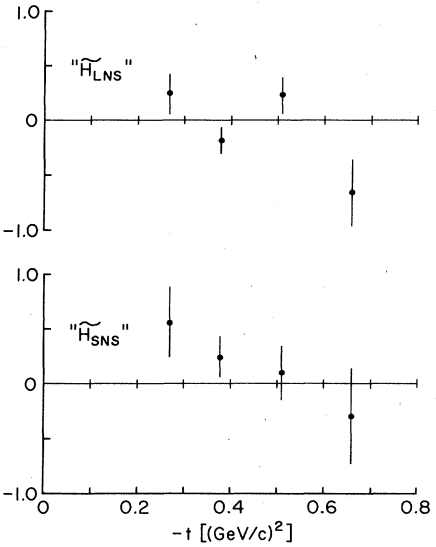

FIG. 10. Spin observables which should vanish or be close to zero from this experiment. Deviations would indicate systematic errors in the data.

$$1-D_{NN}=2(|U_0|^2+|U_2|^2)/\sigma\ ,$$
$$C_{NN}-K_{NN}=4\,\mathrm{Re}U_0U_2^*/\sigma\ .$$

So,

$$1-D_{NN}\geq|C_{NN}-K_{NN}|\ . \tag{14}$$

At $-t\sim0.27$ and 0.38 (GeV/c)^2, the data of Miller *et al.*[10] give $C_{NN}=0.066\pm0.011$ and 0.069 ± 0.014, and from Table V, $K_{NN}=0.134\pm0.045$ and 0.126 ± 0.025, respectively. The relation in Eq. (14) is also shown in Fig. 11 using data from Refs. 2, 9, 10, and 14. Note that 1 and C_{NN} do not depend on A_{pC}, but that K_{NN} and D_{NN} are inversely proportional to the carbon analyzing power.

Defining the rotated spin parameters

$$(\alpha,\beta;0,R)=(\alpha,\beta;0,S)\cos\theta_R+(\alpha,\beta;0,L)\sin\theta_R\ ,$$
$$(\alpha,\beta;0,r)=(\alpha,\beta;0,L)\cos\theta_R-(\alpha,\beta;0,S)\sin\theta_R\ , \tag{15}$$

then additional inequalities similar to Eq. (14) can be derived. For example,

$$1+D_{NN}\geq|C_{NN}+K_{NN}|\ ,$$
$$1+D_{SR}\geq|C_{SS}+K_{SR}|\ ,$$
$$1+D_{SR}\geq|H_{SNr}-H_{SLN}|\ ,$$
$$1-D_{SR}\geq|C_{SS}-K_{SR}|\ ,$$
$$1-D_{SR}\geq|H_{SNr}+H_{SLN}|\ , \tag{16}$$
$$1+D_{Lr}\geq|C_{LL}+K_{Lr}|\ ,$$
$$1+D_{Lr}\geq|H_{LNR}-H_{LSN}|\ ,$$
$$1-D_{Lr}\geq|C_{LL}-K_{Lr}|\ ,$$
$$1-D_{Lr}\geq|H_{LNR}+H_{LSN}|\ .$$

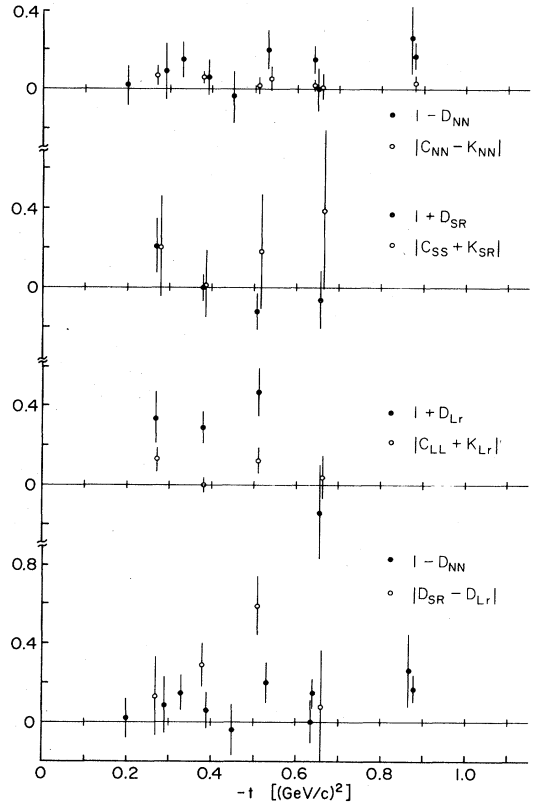

FIG. 11. Several tests for consistency of the data. The quantities in absolute value should be smaller than the corresponding quantities $1\pm D_{ij}$. Data are from Refs. 2, 9–12, 14, and this experiment.

In general, there are insufficient H_{ijk} data to test these expressions. Since D_{SR} and D_{Lr} are both negative, the most stringent tests involve $(1+D_{SR})$ and $(1+D_{Lr})$ in Eqs. (16) above. The values of D_{SR}, D_{Lr}, K_{LR}, etc., are given in Tables VIII and IX and data for the inequalities are shown in Fig. 11 using data from Refs. 11 and 12. [Note that the relations $D_{LR}=-D_{Sr}$, $K_{LR}=-K_{Sr}$, $H_{LNr}=H_{SNR}$, $H_{NLr}=H_{NSR}$ lead to Eqs. (9)–(11), respectively.]

A number of other inequalities can also be derived from the expressions in Table I. For example,

$$1+C_{NN}\geq|C_{SS}-C_{LL}|\ ,$$
$$1+C_{NN}\geq|H_{LSN}+H_{SLN}|\ ,$$
$$1-C_{NN}\geq|C_{SS}+C_{LL}|\ ,$$
$$1-C_{NN}\geq|H_{LSN}-H_{SLN}|\ ,$$
$$1+K_{NN}\geq|K_{SR}+K_{Lr}|\ ,$$
$$1+K_{NN}\geq|H_{SNr}-H_{LNR}|\ , \tag{17}$$
$$1-K_{NN}\geq|K_{SR}-K_{Lr}|\ ,$$
$$1-K_{NN}\geq|H_{SNr}+H_{LNR}|\ ,$$
$$1+D_{NN}\geq|D_{SR}+D_{Lr}|\ ,$$
$$1+D_{NN}\geq|H_{NSr}-H_{NLR}|\ ,$$

$$1-D_{NN} \geq |D_{SR}-D_{Lr}| ,$$

$$1-D_{NN} \geq |H_{NSr}+H_{NLR}| .$$

Again, there are insufficient H_{ijk} data to perform these tests. The fact that C_{NN} and K_{NN} are small means that the corresponding expressions above are not very stringent. Therefore, the only strong test is provided by the $(1-D_{NN})$ equation. This is also shown in Fig. 11 using data from Refs. 2, 9, and 14.

The conclusion from the tests shown in Fig. 11 is that there is little evidence for problems with the carbon analyzing power A_{pC} except for the last inequality at $t=-0.51$. For this point, the discrepancy is 2—3 standard deviations, which may not be statistically significant. In addition to Fig. 11, it should be noted that D_{SL} is significantly below -1.0 at the largest angles. On the other hand, the systematic error on D_{SL} from Table VI is $\pm 33\%$, since (0.24 ± 0.08) D_{SL} is measured (see Table IV).

Figure 12 shows a plot of A_{pC} from a variety of other polarimeters,[24] as well as from this polarimeter measured in Ref. 1. There is a good agreement within the rather sizable errors of Ref. 1. On the other hand, the data summarized in Ref. 24 are not weighted by the differential cross section or acceptance, and they are integrated over scattering angles in the carbon, θ_c, from 6° to 20°, whereas the range was $\theta_c \sim 6°$ to 16° for the polarimeter in this paper.

There are a number of reasons that the recoil-particle energies could be different in Ref. 1 and in these experiments for a given scattering angle in the polarized target. Small alignment errors of the chamber positions could have caused slightly different t ranges in the two cases. There also could have been differences in the location of the beam-spot center within the target flask, since the beam and target could only be aligned within $\pm(1-2)$ mm. This could have affected the recoil-particle energy losses. Finally, the carbon analyzer thickness in Ref. 1 was 1.90 cm at small $|t|$ and 7.62 cm at large $|t|$, whereas it was 5.08 cm at all t in these experiments.

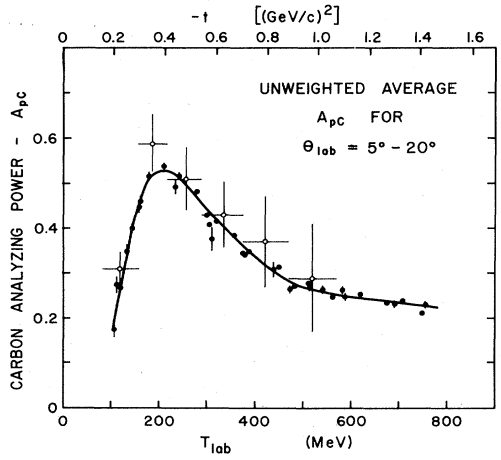

FIG. 12. A comparison of A_{pC} used in Ref. 1 with values from other polarimeters from Ref. 24. The scattering angle in the carbon $\theta_c=\theta_{lab}$ is 5° to 20° from Ref. 24 and is 6° to 16° from Ref. 1.

As a consequence of these differences, the values of A_{pC} used in this experiment have been estimated from Fig. 12 and from the calculated energy losses in the polarized target, carbon, etc. The results are given in Table VII. Compared to Ref. 1, the values are unchanged at $-t=0.51$ and 0.66 $(\mathrm{GeV}/c)^2$, and somewhat lower at $-t=0.38$, 0.83, and 1.00 $(\mathrm{GeV}/c)^2$. A significant difference occurs at $-t=0.27$ $(\mathrm{GeV}/c)^2$ from the thicker carbon used in these experiments. Generous uncertainties on A_{pC} have been assigned to allow for the differences noted above, as well as the effects of the differential cross section and acceptance.

V. AMPLITUDE ANALYSIS

An amplitude analysis was performed using the data in Table V together with existing results.[1-14,25] The amplitudes are normalized so that $\sigma \equiv d\sigma/d\Omega = 1$. The procedure to obtain the amplitudes is described in Ref. 15; it is similar to the method of Ghahramany, Goldstein, and Moravcsik.[26] In the fits, statistical and systematic errors were combined for all data with the exception of the re-

TABLE X. Expressions of some spin observables in terms of exchange amplitudes assuming N_0 dominance. The amplitude N_0 is taken to be much larger in magnitude than all other amplitudes. It is also assumed to be purely positive imaginary.

σ	$\lvert N_0 \rvert^2$
P	$-2\dfrac{\mathrm{Re}N_1}{\lvert N_0 \rvert}$
C_{NN}	$-2\dfrac{\mathrm{Im}N_2}{\lvert N_0 \rvert}$
C_{LL}	$-2\dfrac{\mathrm{Im}U_0}{\lvert N_0 \rvert}$
C_{SS}	$2\dfrac{\mathrm{Im}U_2}{\lvert N_0 \rvert}$
K_{NN}	$-2\dfrac{\mathrm{Im}N_2}{\lvert N_0 \rvert}$
K_{LS}	$-2\dfrac{\mathrm{Im}U_0}{\lvert N_0 \rvert}\sin\theta_R$
D_{SS}	$-2\dfrac{\mathrm{Im}N_1}{\lvert N_0 \rvert}\sin\theta_R - \cos\theta_R$
H_{NSS}	$2\dfrac{\mathrm{Re}N_2}{\lvert N_0 \rvert}\sin\theta_R + 2\dfrac{\mathrm{Re}N_1}{\lvert N_0 \rvert}\cos\theta_R$
H_{LSN}	$-2\dfrac{\mathrm{Re}U_0}{\lvert N_0 \rvert}$
H_{SNS}	$2\dfrac{\mathrm{Re}U_2}{\lvert N_0 \rvert}\sin\theta_R$
H_{SLN}	$-2\dfrac{\mathrm{Re}U_2}{\lvert N_0 \rvert}$

sults in this paper. Even though extensive random searches were performed at all angles, it is not certain that the amplitude solutions found are either unique or correspond to the minimum χ-squared per degree of freedom (χ^2/DF). This is especially true at larger $|t|$, where there are fewer data and the statistical errors are larger.

The results of the amplitude analysis indicate that the amplitude N_0, which is taken to be purely positive imaginary, is dominant. Under these circumstances, the amplitudes can be readily evaluated because the observables can be expressed in the simple forms shown in Table X; the inverse expressions (amplitudes in terms of observables) are shown in Table XI. The derived exchange amplitudes are found in Table XII.

The amplitudes in Table XII are shown with two errors. The first is a "statistical error" corresponding to an

TABLE XI. Expressions of exchange amplitudes in terms of some spin observables assuming N_0 dominance.

Amplitude	Real	Imaginary
$\frac{N_1}{\lvert N_0\rvert}$	$-\frac{P}{2}$	$-\frac{D_{SS}+\cos\theta_R}{2\sin\theta_R}$
$\frac{N_2}{\lvert N_0\rvert}$	$\frac{H_{NSS}+P\cos\theta_R}{2\sin\theta_R}$	$-\frac{K_{NN}}{2}, -\frac{C_{NN}}{2}$
$\frac{U_0}{\lvert N_0\rvert}$	$-\frac{H_{LSN}}{2}$	$-\frac{C_{LL}}{2}, -\frac{K_{LS}}{2\sin\theta_R}$
$\frac{U_2}{\lvert N_0\rvert}$	$-\frac{H_{SLN}}{2}, \frac{H_{SNS}}{2\sin\theta_R}$	$\frac{C_{SS}}{2}$

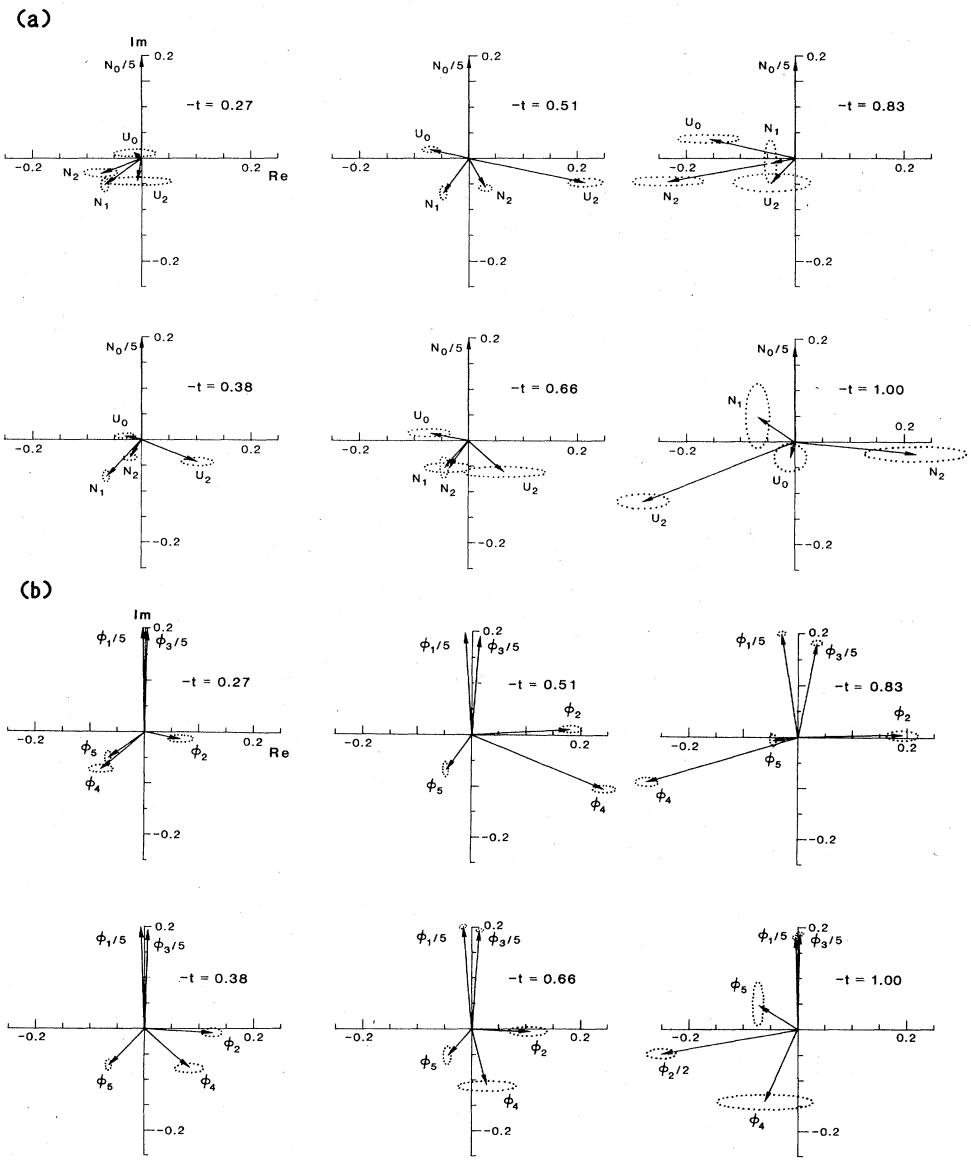

FIG. 13. (a) Scattering amplitudes in exchange channels at $|t|=0.27$ to 1.00 (GeV/c)^2. (b) s-channel helicity amplitudes at $|t|=0.27$ to 1.00 (GeV/c)^2. The amplitudes at $-t=0.83$ and 1.00 (GeV/c)^2 are especially uncertain because of the smaller number of different spin observables measured.

TABLE XII. Exchange amplitudes derived from the world's data for p-p elastic scattering at 6 GeV/c and small $-t$. The amplitude N_0 is assumed to be positive imaginary. The uncertainties on the amplitudes correspond to an increase in χ^2 by a value of 1.0 (statistical only) and to combined statistical and systematic errors. The number of experimental data, the χ^2 per degree of freedom, and the number of different spin observables used in the amplitude determination (excluding $d\sigma/d\Omega$) are also tabulated.

$-t$ [(GeV/c)^2]	0.27	0.38	0.51
ReN_0	0.0	0.0	0.0
ImN_0	0.988 ±0.004±0.015	0.983 ±0.003±0.005	0.964 ±0.007±0.009
ReN_1	−0.068 ±0.003±0.007	−0.064 ±0.002±0.003	−0.047 ±0.002±0.002
ImN_1	−0.051 ±0.015±0.076	−0.071 ±0.009±0.014	−0.067 ±0.012±0.021
ReN_2	−0.073 ±0.032±0.059	−0.021 ±0.012±0.012	+0.031 ±0.011±0.012
ImN_2	−0.029 ±0.006±0.008	−0.035 ±0.006±0.007	−0.058 ±0.004±0.005
ReU_0	−0.012 ±0.038±0.047	−0.030 ±0.014±0.014	−0.071 ±0.013±0.015
ImU_0	+0.009 ±0.006±0.011	+0.008 ±0.002±0.003	+0.018 ±0.003±0.004
ReU_2	−0.007 ±0.060±0.091	+0.103 ±0.029±0.038	+0.213 ±0.031±0.035
ImU_2	−0.044 ±0.006±0.007	−0.043 ±0.005±0.006	−0.047 ±0.005±0.005
No. of data	32	32	32
χ^2/degree of freedom	1.40	1.22	1.43
No. of different spin observables	21	21	21

$-t$ [(GeV/c)^2]	0.66	0.83	1.00
ReN_0	0.0	0.0	0.0
ImN_0	0.987 ±0.005±0.006	0.953 ±0.016±0.017	0.919 ±0.022±0.022
ReN_1	−0.044 ±0.003±0.004	−0.044 ±0.010±0.011	−0.071 ±0.019±0.020
ImN_1	−0.052 ±0.021±0.027	−0.007 ±0.042±0.048	+0.048 ±0.064±0.068
ReN_2	−0.039 ±0.039±0.039	−0.235 ±0.063±0.064	+0.220 ±0.092±0.092
ImN_2	−0.054 ±0.007±0.008	−0.046 ±0.005±0.005	−0.023 ±0.013±0.013
ReU_0	−0.071 ±0.035±0.036	−0.159 ±0.055±0.057	−0.009 ±0.029±0.029
ImU_0	+0.014 ±0.005±0.006	+0.041 ±0.005±0.005	−0.031 ±0.030±0.030
ReU_2	+0.066 ±0.077±0.079	−0.043 ±0.069±0.069	−0.278 ±0.048±0.048
ImU_2	−0.059 ±0.006±0.007	−0.044 ±0.18±0.019	−0.117 ±0.013±0.013
No. of data	35	25	23
χ^2/degree of freedom	1.30	1.80	1.04
No. of different spin observables	21	16	16

increase in χ^2 by 1.0 from the minimum value. The corresponding minimum χ^2/DF is also shown in Table XII, and its value is typically 1.4. The second error corresponds to the inclusion of the systematic uncertainties shown in Table VI. In some cases, this second error is substantially larger than the first error.

If it proves necessary to modify the values in Table V for a different value of carbon analyzing power, they can be scaled as $A_{pC}{}^{-1}$. In particular, it can be shown that the distortion function $\eta(\phi)$ defined in the Appendix is

very insensitive to A_{pC}. For example, the error in the spin parameters in Table V caused by ignoring $\eta(\phi)$ is far less than the statistical uncertainties for changes in A_{pC} by a factor of 2.

The results of the amplitude determination are shown in Fig. 13(a) for the exchange amplitudes and in Fig. 13(b) for the s-channel helicity amplitudes. Note that the magnitudes of N_0, ϕ_1, and ϕ_3 are scaled down a factor of 5 in Fig. 13.

VI. INTERPRETATION

Although there have been extensive measurements, p-p elastic scattering at high energies remains one of the least understood processes. Even with its large cross section at small angles and its symmetry properties, the complexities associated with five scattering amplitudes, and the experimental difficulties of performing many different spin measurements to determine these amplitudes, have limited the detailed knowledge on this reaction.

For example, it was generally expected that N_0 is the dominant amplitude at small angles.[27–30] However, in spite of all the experiments at 6 GeV/c prior to these measurements,[1–14] the dominance of the N_0 amplitude was not well established.[31–33] With the new data in this paper, N_0 dominance at small angles now appears to be experimentally verified, as shown in Fig. 13 (assuming our search found the correct amplitude solution).

Several approaches have been used in the past to study the spin structure of the amplitudes from the 6-GeV/c data in Refs. 1–14. The most standard approach has been the use of the Regge-pole-exchange model. Berger, Irving, and Sorensen[27] have used such a model with parameters determined from other reactions, as well as p-p elastic scattering at various energies, to predict the p-p amplitudes at 6 and 12 GeV/c. Their work is generally considered the standard model in this field. Kroll, Leader, and von Schlippe[28] have used dispersion-theoretic calculations, information from other reactions, and some "physically reasonable assumptions" about some of the helicity-flip amplitudes to compute the p-p amplitudes at 6 GeV/c. Wakaizumi and Sawamoto[29] have investigated the p-p interaction at 6 and 12 GeV/c at all angles using the impact parameter representation and the eikonal model. Fits to previous data allowed conclusions on the magnitudes of the short-, medium-, and long-range components of the spin-dependent eikonals. Finally, semiphenomenological phase-shift analyses[30] have been performed at 6 GeV/c using data from Refs. 1–14 as well as total and differential cross sections.

In general, there is fair agreement between the amplitude analyses in Refs. 27–30 and the amplitudes given in Fig. 13. The absolute phase of N_0 is slightly different in these models. Since this phase cannot be determined with the present data, N_0 will be taken to be purely positive imaginary in the discussion below. At $|t|=0.38$ $(\mathrm{GeV}/c)^2$ the largest disagreements between predictions and the observed amplitudes occur for $\mathrm{Im}(N_1)$, where Berger *et al.*[27] have positive values and Wakaizumi and Sawamoto[29] have more negative values than Fig. 13; for $\mathrm{Re}(N_2)$, where Kroll, Leader, and von Schlippe[28] have positive values while Fig. 13 shows slightly negative results; and for $\mathrm{Im}(N_2)$, where Matsuda *et al.*[30] predict positive values and Fig. 13 has negative values. There is rough agreement on the magnitude and phase for U_0 and U_2 between these models and the amplitudes in Fig. 13; however, the magnitude of N_0 is observed to be somewhat smaller than the model predictions.

Moravcsik, Goldstein, and co-workers have commented on p-p elastic scattering at 6 GeV/c in many articles.[26,32–36] Several papers deal with the problem of how best to determine the amplitudes.[26,32] An extensive amplitude analysis from $-t=0.05$ to 1.0 $(\mathrm{GeV}/c)^2$ has also been performed.[26,34] Four different solutions with approximately the same χ^2/DF were found; set 3 seems closest to the results in Fig. 13. A comparison of these solutions to the Regge-pole-exchange model of Berger *et al.*[27] is given in Ref. 33. Polarization tests of one-particle-exchange mechanisms have been applied to the 6-GeV/c amplitudes and have been shown to be satisfied, whereas they fail at lower energies.[35] Finally, these authors also interpret the results for the 6-GeV/c in the framework of QCD.[36] In particular, the data show that the spin-nonflip helicity amplitudes ϕ_1 and ϕ_3 are much larger than the spin-flip amplitudes. This indicates that helicity conserving exchange terms are dominant, as would be the case if exchanged gluons couple to current quarks in the nucleons.

The amplitude picture seems easier to understand in terms of the s-channel helicity amplitudes, where little variation is observed in ϕ_1, ϕ_3, and ϕ_5 over most of the t range of this experiment. As noted above, the dominant amplitudes are $\phi_1 \simeq \phi_3$. In addition, the ϕ_2 amplitude remains almost (relatively) real up to $|t|=1.0$ $(\mathrm{GeV}/c)^2$, though there is a change in its magnitude and direction. There is, however, a large variation in both the magnitude and direction of ϕ_4. As has been noted by Kroll *et al.*,[28] "surprisingly, the most interesting structure is in ϕ_2 and ϕ_4 themselves rather than in the combinations" N_2 and U_2. It is hoped that these measurements will stimulate further work to understand this structure in the helicity double-flip amplitudes.

VII. CONCLUSIONS

New experimental results on double- and triple-scattering spin parameters in p-p elastic scattering at 6 GeV/c are presented. These allow the first nucleon-nucleon amplitude determination in the multi-GeV range, where a model-independent analysis is the only reliable method to obtain the amplitudes at present. These results are consistent with dominance of the spin-nonflip helicity amplitudes (ϕ_1,ϕ_3,N_0) at all $|t|$ from 0.27 to 1.0 GeV^2/c^2. A search for amplitudes that correspond to all 6-GeV/c spin data yielded the results shown in Fig. 13. Even though many searches were performed, it is not certain that the amplitudes in Fig. 13 are either unique or correspond to the minimum χ^2/DF. This is especially true at $-t=0.83$ and 1.00 $(\mathrm{GeV}/c)^2$, where there are fewer data and larger statistical errors.

Many tests for systematic errors were performed, as

well as a number of consistency checks. In general, the data are internally consistent, although there are a few cases where 2—3 standard deviation discrepancies occur. Various tests indicate agreement with previous data, except that the new D_{SS} values may be slightly smaller in magnitude than the data in Ref. 5. Various differences from Ref. 1 led to the adoption of carbon-analyzing power (A_{pC}) values from measurement with other polarimeters.[24] Particularly uncertain is A_{pC} at $t=-0.27$ $(\mathrm{GeV}/c)^2$. We encourage a remeasurement of some spin parameters at this angle to reduce the uncertainty on A_{pC} and consequently on the amplitudes.

ACKNOWLEDGMENTS

We wish to acknowledge the assistance of Dr. C. Chang-Fang and Dr. P. Rynes during the data analysis, and R. Daly, O. Fletcher, F. Paulis, B. Millar, W. Haberichter, T. Kasprzyk, and A. Rask during the data-taking periods. We also express appreciation to the Zero Gradient Synchrotron operations staff. Finally we wish to thank Dr. E. Berger, Dr. G. Thomas, Dr. C. Sorensen, and other members of the ANL theory group and Dr. M. Moravcsik and Dr. G. Goldstein for many useful discussions on these data. This work was supported in part by the U.S. Department of Energy.

APPENDIX

Recoil protons from elastic scatterings on the PPT were binned into intervals in t (four-momentum transfer squared). The azimuthal distribution for recoil protons elastically scattered by the carbon in the polarimeter can then be written

$$N^{\pm\pm}(\phi_i)=\eta(\phi_i)I_0[1+a_0^{\pm\pm}-a_N^{\pm\pm}\sin(\phi_i-\phi_N)-a_L^{\pm\pm}\sin(\phi_i-\phi_L)-a_S^{\pm\pm}\sin(\phi_i-\phi_S)]\ , \tag{A1}$$

where superscripts $\pm\pm$ indicate the polarities of the beam and the target polarizations. The coefficients a_i may be expressed in terms of observables according to

$$\begin{aligned}
a_0&=(\alpha_N P_B+\beta_N P_T)P+P_B P_T[\alpha_N\beta_N C_{NN}+\alpha_L\beta_L C_{LL}+\alpha_S\beta_S C_{SS}+(\alpha_L\beta_S+\alpha_S\beta_L)C_{LS}]\ ,\\
a_N&=A_{pC}\gamma_N[P+\alpha_N P_B K_{NN}+\beta_N P_T D_{NN}+P_B P_T(\alpha_N\beta_N P+\alpha_L\beta_S H_{LSN}+\alpha_L\beta_L H_{LLN}+\alpha_S\beta_L H_{SLN}+\alpha_S\beta_S H_{SSN})]\ ,\\
a_L&=A_{pC}\gamma_L[P_B(\alpha_L K_{LL}+\alpha_S K_{SL})+P_T(\beta_L D_{LL}+\beta_S D_{SL})+P_B P_T(\alpha_N\beta_L H_{NLL}+\alpha_N\beta_S H_{NSL}+\alpha_L\beta_N H_{LNL}+\alpha_S\beta_N H_{SNL})]\ ,\\
a_S&=A_{pC}\gamma_S[P_B(\alpha_L K_{LS}+\alpha_S K_{SS})+P_T(\beta_L D_{LS}+\beta_S D_{SS})+P_B P_T(\alpha_N\beta_L H_{NLS}+\alpha_N\beta_S H_{NSS}+\alpha_L\beta_N H_{LNS}+\alpha_S\beta_N H_{SNS})]\ ,
\end{aligned} \tag{A2}$$

where A_{pC} is the analyzing power of the carbon polarimeter; the other parameters are defined in the text. Spin parameters such as H_{SNN} disappear because of the symmetry properties of elastic p-p scattering.

Terms in Eq. (A1) involving P_B, P_T, and $P_B P_T$ can be combined so that

$$N^{\pm\pm}(\phi_i)=\eta(\phi_i)I_0[X_0(\phi_i)+P_B^{\pm\pm}X_B(\phi_i)+P_T^{\pm\pm}X_T(\phi_i)+(P_B P_T)^{\pm\pm}X_{BT}(\phi_i)]\ , \tag{A3}$$

with

$$\begin{aligned}
X_0&=1-A_{pC}\gamma_N P\sin(\phi_i-\phi_N)\ ,\\
X_B&=\alpha_N P-A_{pC}[\gamma_N\alpha_N K_{NN}\sin(\phi_i-\phi_N)+\gamma_L(\alpha_L K_{LL}+\alpha_S K_{SL})\sin(\phi_i-\phi_L)+\gamma_S(\alpha_L K_{LS}+\alpha_S K_{SS})\sin(\phi_i-\phi_S)]\ ,\\
X_T&=\beta_N P-A_{pC}[\gamma_N\beta_N D_{NN}\sin(\phi_i-\phi_N)+\gamma_L(\beta_L D_{LL}+\beta_S D_{SL})\sin(\phi_i-\phi_L)+\gamma_S(\beta_L D_{LS}+\beta_S D_{SS})\sin(\phi_i-\phi_S)]\ ,\\
X_{BT}&=\alpha_N\beta_N C_{NN}+\alpha_L\beta_L C_{LL}+\alpha_S\beta_S C_{SS}+(\alpha_L\beta_S+\alpha_S\beta_L)C_{LS}\\
&\quad -A_{pC}[\gamma_N(\alpha_N\beta_N P+\alpha_L\beta_S H_{LSN}+\alpha_L\beta_L H_{LLN}+\alpha_S\beta_L H_{SLN}+\alpha_S\beta_S H_{SSN})\sin(\phi_i-\phi_N)\\
&\quad +\gamma_L(\alpha_N\beta_L H_{NLL}+\alpha_N\beta_S H_{NSL}+\alpha_L\beta_N H_{LNL}+\alpha_S\beta_N H_{SNL})\sin(\phi_i-\phi_L)\\
&\quad +\gamma_S(\alpha_N\beta_L H_{NLS}+\alpha_N\beta_S H_{NSS}+\alpha_L\beta_N H_{LNS}+\alpha_S\beta_N H_{SNS})\sin(\phi_i-\phi_S)]\ .
\end{aligned} \tag{A4}$$

Equation (A3) may be expressed in matrix form

$$\begin{bmatrix} N^{++}\\ N^{-+}\\ N^{+-}\\ N^{--}\end{bmatrix}=\eta I_0 M_{\mathrm{pol}}\begin{bmatrix} X_0\\ X_B\\ X_T\\ X_{BT}\end{bmatrix}\ , \tag{A5}$$

with

$$M_{\mathrm{pol}}=\begin{bmatrix} 1 & P_B{}^{++} & P_T{}^{++} & (P_B P_T)^{++}\\ 1 & P_B{}^{-+} & P_T{}^{-+} & (P_B P_T)^{-+}\\ 1 & P_B{}^{+-} & P_T{}^{+-} & (P_B P_T)^{+-}\\ 1 & P_B{}^{--} & P_T{}^{--} & (P_B P_T)^{--}\end{bmatrix}\ , \tag{A6}$$

where explicit dependence on the angle ϕ_c has been suppressed. Inverting Eq. (A6) we obtain

$$\eta I_0 \begin{bmatrix} X_0 \\ X_B \\ X_T \\ X_{BT} \end{bmatrix} = M_{\text{pol}}{}^{-1} \begin{bmatrix} N^{++} \\ N^{-+} \\ N^{+-} \\ N^{--} \end{bmatrix} , \tag{A7}$$

where the right-hand side of the equation depends only on the experimental data.

The first component of the vector X in Eq. (A5) is

$$X_0^{\text{cal}}(\phi_i) = 1 - A_{pC}\gamma_N P \sin(\phi_i - \phi_N) , \tag{A8}$$

which can be independently calculated for each ϕ_i bin using existing polarization data and calculated values for the parameters γ_N and ϕ_N.

A new vector, X^{expt}, may also be defined using only the experimental data

$$\begin{bmatrix} X_0^{\text{expt}} \\ X_B^{\text{expt}} \\ X_T^{\text{expt}} \\ X_{BT}^{\text{expt}} \end{bmatrix} = M_{\text{pol}}{}^{-1} \begin{bmatrix} N^{++} \\ N^{-+} \\ N^{+-} \\ N^{--} \end{bmatrix} \Big/ I_0 . \tag{A9}$$

The distortion function is then obtained directly,

$$\eta(\phi_i) = X_0^{\text{expt}}(\phi_i)/X_0^{\text{cal}}(\phi_i) . \tag{A10}$$

For the present analysis, $\eta(\phi_i)$ was fitted by a polynomial function

$$\eta(\phi) = \sum_0^3 C_n \cos^n\phi + \sum_1^3 S_n \sin^n\phi . \tag{A11}$$

With this function, the corrected distribution becomes

$$X_k(\phi_i) = \frac{X_k^{\text{expt}}(\phi_i)}{\eta(\phi_i)} \; ; \; k = B \; , \; T, \text{ and } BT . \tag{A12}$$

Using available data for P, C_{NN}, C_{LL}, C_{SS}, and C_{LS} we can generate another set of azimuthal distributions without constant terms:

$$\begin{aligned} n^{(1)}(\phi_i) &= 1 - X_0(\phi_i) , \\ n^{(2)}(\phi_i) &= \alpha_N P - X_B(\phi_i) , \\ n^{(3)}(\phi_i) &= \beta_N P - X_T(\phi_i) , \\ n^{(4)}(\phi_i) &= \alpha_N\beta_N C_{NN} + \alpha_L\beta_L C_{LL} + \alpha_S\beta_S C_{SS} \\ &\quad + (\alpha_L\beta_S + \alpha_S\beta_L)C_{LS} - X_{BT}(\phi_i) . \end{aligned} \tag{A13}$$

These expressions can be expressed explicitly through the single-, double-, and triple-spin parameters as

$$\begin{aligned} n^{(1)}(\phi) &= A_{pC}\gamma_N P \sin(\phi - \phi_N) , \\ n^{(2)}(\phi) &= A_{pC}[\gamma_N\alpha_N K_{NN}\sin(\phi - \phi_N) + \gamma_L(\alpha_L K_{LL} + \alpha_S K_{SL})\sin(\phi - \phi_L) + \gamma_S(\alpha_L K_{LS} + \alpha_S K_{SS})\sin(\phi - \phi_S)] , \\ n^{(3)}(\phi) &= A_{pC}[\gamma_N\beta_N D_{NN}\sin(\phi - \phi_N) + \gamma_L(\beta_L D_{LL} + \beta_S D_{SL})\sin(\phi - \phi_L) + \gamma_S(\beta_L D_{LS} + \beta_S D_{SS})\sin(\phi - \phi_S)] , \\ n^{(4)}(\phi) &= A_{pC}[\gamma_N(\alpha_N\beta_N P + \alpha_L\beta_S H_{LSN} + \alpha_L\beta_L H_{LLN} + \alpha_S\beta_L H_{SLN} + \alpha_S\beta_S H_{SSN})\sin(\phi - \phi_N) \\ &\quad + \gamma_L(\alpha_N\beta_L H_{NLL} + \alpha_N\beta_S H_{NSL} + \alpha_L\beta_N H_{LNL} + \alpha_S\beta_N H_{SNL})\sin(\phi - \phi_L) \\ &\quad + \gamma_S(\alpha_N\beta_L H_{NLS} + \alpha_N\beta_S H_{NSS} + \alpha_L\beta_N H_{LNS} + \alpha_S\beta_N H_{SNS})\sin(\phi - \phi_S)] . \end{aligned} \tag{A14}$$

The first combination, $n^{(1)}$, has already been used in the evaluation of the distortion function $\eta(\phi)$. The other three combinations can be fitted with

$$\begin{aligned} n^{(j)}(\phi) &= A^{(j)}\sin\phi - B^{(j)}\cos\phi \\ &= C^{(j)}\sin(\phi - \phi_0^{(j)}) . \end{aligned} \tag{A15}$$

In principle, the spin parameters of interest may now be obtained from the fitted values of the $A^{(j)}$ and $B^{(j)}$. However, with limited data this procedure is impractical if the expressions for $n^{(j)}$ in Eq. (A13) contain more than two parameters significantly different from zero. In the present experiment, beam and target polarizations were usually aligned so that only one α and one β were significantly different from zero (see Tables II and III); the γ and ϕ parameters depend on the momentum of the recoil proton as shown in Fig. 6. Coefficients of spin parameters which contribute to the azimuthal distributions are listed in Table IV. In each case there are only two large terms which contribute to the expressions for $n^{(j)}(\phi)$ in Eq. (A14).

With this simplification, the equation

$$A\sin\phi - B\cos\phi = C_1\sin(\phi - \phi_1) + C_2\sin(\phi - \phi_2) \tag{A16}$$

gives the spin parameters of interest; here ϕ_1 and ϕ_2 are the projected angles in the X'-Y' plane for the respective spin directions. Then

$$\begin{aligned} C_1 &= \frac{A\sin\phi_2 - B\cos\phi_2}{\sin(\phi_2 - \phi_1)} , \\ C_2 &= \frac{-A\sin\phi_1 + B\cos\phi_1}{\sin(\phi_2 - \phi_1)} , \\ \Delta C_1 &= \frac{[(\sin\phi_2\Delta A)^2 + (\cos\phi_2\Delta B)^2]^{1/2}}{\sin(\phi_2 - \phi_1)} , \\ \Delta C_2 &= \frac{[(\sin\phi_1\Delta A)^2 + (\cos\phi_1\Delta B)^2]^{1/2}}{\sin(\phi_2 - \phi_1)} . \end{aligned} \tag{A17}$$

The final result is obtained by dividing these expressions by the analyzing power and the appropriate coefficient listed in Table IV.

[a]Present address: Bell Telephone Laboratories, Holmdel, NJ 07733.
[b]Research participant: Louisville University, Louisville, KY 40292.
[c]Present address: Los Alamos National Laboratory, Los Alamos, NM 87545.
[d]Present address: Energy and Environmental Systems Division, Argonne National Laboratory, Argonne, IL 60439.
[e]Present address: 5336 S. University Ave., Chicago, IL 60615.
[f]Present address: Motorola Communications Systems Division, Franklin Park, IL 60131.
[g]Present address: General Electric Company, Medical Systems Division, Milwaukee, WI 53201.
[h]Present address: Kyoto University, Kyoto 606, Japan.
[i]Present address: KEK, Tsukuba, Ibaraki 305, Japan.
[j]Present address: Rutgers University, Piscataway, NJ 08854.

[1]A. Beretvas *et al.*, Phys. Rev. D **20**, 21 (1979).
[2]R. C. Fernow *et al.*, Phys. Lett. **52B**, 243 (1974); J. R. O'Fallon *et al.*, Phys. Rev. Lett. **32**, 77 (1974); L. G. Ratner *et al.*, Phys. Rev. D **15**, 604 (1977); M. Borghini *et al.*, *ibid.* **17**, 24 (1978).
[3]P. Grannis *et al.*, Phys. Rev. **148**, 1297 (1966).
[4]M. Borghini *et al.*, Phys. Lett. **24B**, 77 (1966); **31B**, 405 (1970); **31B**, 405(E) (1970); M. Borghini (private communication).
[5]J. Deregel *et al.*, Phys. Lett. **43B**, 338 (1973); Nucl. Phys. **B103**, 269 (1976).
[6]G. W. Abshire *et al.*, Phys. Rev. Lett. **32**, 1261 (1974).
[7]R. Diebold *et al.*, Phys. Rev. Lett. **35**, 632 (1975).
[8]D. R. Rust *et al.*, Phys. Lett. **58B**, 114 (1975).
[9]G. W. Abshire *et al.*, Phys. Rev. D **12**, 3393 (1975).
[10]D. Miller *et al.*, Phys. Rev. Lett. **36**, 763 (1976); Phys. Rev. D **16**, 2016 (1977).
[11]I. P. Auer *et al.*, Phys. Rev. Lett. **37**, 1727 (1976).
[12]I. P. Auer *et al.*, Phys. Lett. **70B**, 475 (1977).
[13]R. D. Klem *et al.*, Phys. Rev. D **15**, 602 (1977).
[14]H. Courant *et al.*, Phys. Rev. Lett. **44**, 1373 (1980).
[15]P. W. Johnson, R. C. Miller, and G. H. Thomas, Phys. Rev. D **15**, 1895 (1977); P. W. Johnson and G. H. Thomas, *ibid.* **16**, 2783 (1977).
[16]E. Leader and R. Slansky, Phys. Rev. **148**, 1491 (1966); E. Leader, *ibid.* **166**, 1599 (1968).
[17]F. Halzen and G. H. Thomas, Phys. Rev. D **10**, 344 (1974).
[18]M. L. Goldberger *et al.*, Phys. Rev. **120**, 2250 (1960).
[19]M. Jacob and G. C. Wick, Ann. Phys. (N.Y.) **7**, 404 (1959).
[20]C. Bourrely, E. Leader, and J. Soffer, Phys. Rep. **59**, 95 (1980).
[21]J. Bystricky, F. Lehar, and P. Winternitz, J. Phys. (Paris) **39**, 1 (1978).
[22]G. H. Thomas, Ph.D. thesis, UCLA, 1969.
[23]E. Colton *et al.*, Nucl. Instrum. Methods **151**, 85 (1978).
[24]R. D. Ransome *et al.*, Nucl. Instrum. Methods **201**, 315 (1982); M. W. McNaughton *et al.* (unpublished).
[25]Complete tables of the input data to the amplitude analysis are available on request. Some unpublished results from our experiments have also been included. These are $\tilde{C}_{SL}=0.951C_{SL}+0.298C_{SS}=-0.0224\pm0.0037$, -0.0246 ± 0.0045, -0.0270 ± 0.0064, -0.0230 ± 0.071, -0.0304 ± 0.0093, and -0.0469 ± 0.0118 at $-t=0.27$, 0.38, 0.51, 0.66, 0.83, and 1.00 $(\mathrm{GeV}/c)^2$, respectively, and $\tilde{C}_{LL}=0.951C_{LL}+0.298C_{LS}=-0.0282\pm0.0089$, -0.0478 ± 0.0066, and -0.0490 ± 0.0084 at $-t=0.66$, 0.83, and 1.00 $(\mathrm{GeV}/c)^2$, respectively.
[26]N. Ghahramany, G. R. Goldstein, and M. J. Moravcsik, Phys. Rev. D **28**, 1086 (1983).
[27]E. L. Berger, A. C. Irving, and C. Sorensen, Phys. Rev. D **17**, 2971 (1978); **23**, 2807(E) (1981).
[28]P. Kroll, E. Leader, and W. von Schlippe, J. Phys. G **4**, 1003 (1978).
[29]S. Wakaizumi and M. Sawamoto, Prog. Theor. Phys. **64**, 1699 (1980); S. Wakaizumi, *ibid.* **67**, 531 (1982).
[30]M. Matsuda *et al.*, Prog. Theor. Phys. **62**, 1436 (1979); **64**, 1344 (1980).
[31]G. H. Thomas, Argonne National Laboratory Report No. ANL-HEP-CP-75-3, 1975 (unpublished).
[32]G. R. Goldstein and M. J. Moravcsik, Phys. Lett. **102B**, 189 (1981); Ann. Phys. (N.Y.) **142**, 219 (1982); K. Nam, M. J. Moravcsik, and G. R. Goldstein, Phys. Rev. Lett. **52**, 2305 (1984).
[33]M. J. Moravcsik, N. Ghahramany, and G. R. Goldstein, Phys. Rev. D **30**, 1899 (1984).
[34]N. Ghahramany, M. J. Moravcsik, and G. R. Goldstein, Phys. Rev. D **31**, 195 (1985).
[35]G. R. Goldstein and M. J. Moravcsik, Phys. Rev. D **30**, 55 (1984); G. R. Goldstein, M. J. Moravcsik, R. Arash, and H. Ghahramany, Phys. Lett. **152B**, 265 (1985).
[36]G. R. Goldstein and M. J. Moravcsik (unpublished).